Diamond synthesis "The science"
A theoretical and experimental study

Ion C. Benea, Ph.D.
Engis Corporation
Wheeling IL 60090, USA

Abstract

Sixty-five years ago, on December 16, 1954, the first repeatable diamond synthesis was successfully achieved by H. T. Hall of General Electric.
Nowadays, billions of carats of diamond powders are produced annually worldwide, based on the high pressure-high temperature catalytic diamond synthesis process.
Although, the pressure-temperature conditions needed for diamond synthesis can be easily established, the mechanism of high pressure-high temperature catalytic transformation of graphite to diamond, remains insufficiently understood. Over time, both published and, unpublished theoretical and experimental studies on graphite-diamond polymorphic transformation have been performed by many.
This work, one of many, proposes a theoretical approach to catalytic diamond synthesis, by way of a mathematical model, with the purpose of understanding the mechanism of the catalytic transformation of graphite to diamond in the binary Carbon-Metal (C-Me) systems with eutectic, at high pressure and high temperature (HP-HT).
The results of mathematical calculations were verified against published experimental data for C-Ni system, and experimental results acquired through diamond synthesis experiments designed to: a) ascertain the pressure-temperature conditions required for diamond formation in C-Co system, and b) establish the effect of pressure and temperature on the nucleation and growth rates that control the physical and chemical properties of synthesized diamond crystals.
Validity of the mathematical model developed was substantiated by the agreement between theoretical calculations and experimental results.
Understanding the mechanism that governs the HP-HT catalytic transformation of graphite to diamond, represents a valuable approach toward an efficient control of the diamond synthesis processes.

1. Phase diagram of carbon

Phase diagram of carbon has risen continuous interest from worldwide scientists, especially after successful production of synthetic diamond by General Electric, USA in 1955. (1)
The phase diagram of carbon, presented in the approximate diagram of Fig. 1.1, represents the summation of all known data pertaining to elemental carbon over a wide range of pressures and temperatures.
The main boundaries between different carbon phases are *graphite/diamond equilibrium line; graphite/liquid equilibrium line* and *diamond/liquid equilibrium line*.

2. Proposed mechanism for HP-HT catalytic transformation of graphite to diamond

It is well known that HP-HT conversion of graphite to diamond involves the presence of a metal in molten state.

There are a number of hypothesis regarding the role metal plays in the conversion process of graphite to diamond (2, 3, 4, 5 – 24).

Of those, solvent-catalyst hypothesis (3, 10, 16, 17, 20) was taken into consideration for the development of a mathematical model for the high pressure-high temperature catalytic transformation of graphite to diamond.

This model assumes that high pressure-high temperature transformation of graphite to diamond is a two-step process: ***nucleation*** *– formation of diamond nuclei, as a result of a solid-solid catalytic transformation process, and* ***growth*** *– growth of diamond crystals by carbon deposition onto existing diamond nuclei, through a diffusion process*.

Under favorable pressure-temperature conditions for thermodynamic stability of diamond, graphite dissolves in metal catalyst with formation of carbon-metal solution. Metal atoms and clusters penetrate graphite lattice and, when in close proximity with carbon atoms, partially filled electronic sub-shell *d* of metal will receive delocalized electrons from the weak π bond of graphite. As a result of loss of electrons from π bond, σ bond becomes weaker and the structure will break into free carbon atoms and carbon clusters with graphitic structure. Graphite dissolution in molten metal continues until carbon reaches equilibrium concentration corresponding to pressure-temperature conditions at which carbon-metal system is submitted to. As a result of energetic (thermodynamic) fluctuations in the carbon-metal solution, carbon atoms and carbon clusters exist in dynamic transitional states – sp^2 hybridization (trigonal-planar geometry) $\rightleftarrows$ sp^3 hybridization (tetrahedral geometry). Some of the carbon clusters with graphitic structure experience a solid-solid catalytic transformation to diamond structure - homogeneous nucleation. This transformation is associated with transition of carbon atoms from sp^2 hybridization to sp^3 hybridization, with rearrangement of the weak graphite structure into diamond structure, through formation of covalent bonding on sp^3 hybrid orbitals between carbon atoms (σ bonds*)*.

Furthermore, carbon-metal intermediate compounds (interstitial solid solutions and/or interstitial compounds) can also be formed between graphite mono-layers and metal atoms.

In addition to spontaneous formation of diamond nuclei, formation of nonspontaneous diamond nuclei in the carbon-metal solution is also possible (heterogenous nucleation). Solid particles of carbon-metal intermediate compounds, high melting point impurities, etc., can become diamond nucleation sites.

If energetic equilibrium in the carbon-metal solution is favorable to diamond growth (pressure-temperature conditions inside the thermodynamic stability domain of diamond), carbon atoms and clusters head toward existing diamond nuclei, driven by the difference in solubility limits between diamond + liquid/liquid boundary and graphite + liquid/liquid boundary.

Given that under these conditions the solubility of graphite in molten metal is higher than that of diamond, carbon-metal solution becomes oversaturated with carbon, prompting deposition of carbon atoms and clusters with sp^3 hybridization onto diamond nuclei. As a result, diamond

crystal starts to develop from diamond nuclei. Following precipitation of carbon atoms and clusters onto diamond nuclei, carbon concentration in carbon-metal solution around newly grown diamond crystal, is reduced. Hence, more carbon atoms and clusters with graphitic structure are dissolved into carbon-metal solution until carbon concentration reaches oversaturation limit again. At the same time, more carbon atoms and clusters in sp^2 hybridization state are activated to sp^3 hybridization state.
Crystal growth process continues for as long as carbon atoms and clusters in sp^3 hybridization state are present in the carbon-metal solution surrounding the newly grown diamond crystal.
If, on the other hand, the energetic equilibrium changes and becomes favorable to graphite growth (pressure-temperature conditions outside the thermodynamic stability domain of diamond), crystal growth process is reversed into diamond dissolution process. Diamond crystal dissolves in metal catalyst simultaneously with deactivation of carbon atoms and clusters from sp^3 hybridization state to sp^2 hybridization state, rearrangement in graphite structure, and formation of graphite nuclei. Under these conditions, the solubility of diamond in molten metal is higher than that of graphite, and carbon-metal solution becomes oversaturated with carbon, prompting deposition of carbon atoms and clusters with sp^2 hybridization onto graphite nuclei.
According to this mechanism, in the HP-HT catalytic transformation of graphite to diamond, the function of metal is preponderantly catalytic, in the process of $sp^2 \rightarrow sp^3$ activation of carbon atoms and clusters and formation of diamond nuclei, based on spontaneous graphite-diamond polymorphic transformation, while in the dissolution of graphite and diamond growth processes, the function of the metal is preponderantly that of carbon solvent.
Thus, mathematical modeling of HP-HT graphite-diamond catalytic transformation in the binary systems C-Me, presumes calculation of pressure-temperature conditions required for the thermodynamic stability of diamond (thermodynamic calculations), as well as calculation of nucleation and growth rates (kinetics calculations) that are responsible for physical and chemical properties of diamond crystals.
With the exception of Fe, at atmospheric pressure, group VIII metals, known as effective catalysts for conversion of graphite to diamond, form with C simple solution systems with eutectic. In this work, mathematical calculations related to solid-liquid thermodynamic equilibrium, were limited to C-Me systems with eutectic, particularly to C-Ni and C-Co systems.

3. Mathematical model for HP-HT catalytic graphite-diamond transformation in binary carbon-metal systems with eutectic

Thermodynamics of phase equilibrium in C-Me systems at high pressure

Peters (25) and Dickinson (26), calculated phase diagrams of C-Ni, C-Co, C-Mn and C-Fe at high pressure and indicated the pressure-temperature conditions for thermodynamic stability of diamond in these systems.
Comparison between the results of theoretical calculations performed by Peters and Dickinson for C-Ni phase diagram at high pressure, with experimental data obtained by Strong (27) for same system, shows that calculated pressure-temperature values are approx. 0.5 GPa and approx. 100 K higher than experimental data. Particularly, the equilibrium temperature calculated for graphite/diamond/liquid equilibrium at a given pressure, exceeds the calculated temperature of

graphite/diamond equilibrium at same given pressure, based on the mathematical relation proposed by Berman and Simon (28) for graphite/diamond equilibrium line, that is well verified experimentally:

$$P\ (GPa) = 0.6865 + 0.00266\ T\ (K) \qquad (3.1)$$

Analyzing the reasons for the erroneous calculations by Peters and Dickenson, we concluded that the mathematical relation chosen for the excess free energy, E_G, of a regular carbon-metal (C-Me) solution used in their calculations, is independent of pressure and temperature.

$$E^f_G(X) = X^f_{Me} * X^f_C * E^{(0)} \qquad (3.2)$$

where:
f: hc; vcc; fcc, or L;
X_{Me} is concentration of metal in carbon-metal solution;
X_C is concentration of carbon in carbon-metal solution;
E = constant.

To calculate the solid/liquid equilibrium diagrams of C-Me systems at high pressure, we chose a mathematical relation for the excess free energy of C-Me solution which is dependent of concentration, X, pressure, P, and temperature, T, as follows:

$$E^f_G = X^f_{Me} * X^f_C\ [E^{(0)}_1 - TE^{(0)}_2 + P(E^{(i)}_1 + E^{(i)}_2)] \qquad (3.3)$$

where:
$E^{(f)}_G$ is the excess free energy;
$E^{(0)}_1$ is the excess enthalpy in phase f;
$E^{(0)}_2$ is the excess enthropy in phase f;
$E^{(i)}_1 + P\ E^{(i)}_2$ is the excess volume in phase f and is dependent of pressure.

For a polymorphic transformation, phase equilibrium between two phases at temperature T and pressure P, implies equality between their respective free energies:

$$G_1 = G_2, \text{ or } \Delta G = \Delta H - T\Delta S + PV = 0 \qquad (3.4)$$

To describe the solid/liquid phase equilibrium in a binary system C-Me with eutectic, at high pressure, the following thermodynamic relations were used in our calculations:

<u>Me^{fcc} – Liquid equilibrium line</u>:

$$\Delta G_{Me}^{fcc/L}(X,T,P) = \Delta^0 H_{Me}^{fcc/L} - T\Delta^0 S_{Me}^{fcc/L} + P\Delta^0 V_{Me}^{fcc/L} + RT \ln (X^L_{Me}) + (1-X^L_{Me})^2[(L_1^{(0)} - T*L_2^{(0)}) + P(L_1^{(1)} + PL_2^{(1)})] = 0 \qquad (3.5.a)$$

<u>Graphite – Liquid equilibrium line</u>:

$$\Delta G_C^{G/L}(X,T,P) = \Delta^0 H_C^{G/L} - T\Delta^0 S_C^{G/L} + P(K_1^{(2)} + PK_2^{(2)}) + RT \ln X_C^L + (1- X_C^L)^2[L_1^{(0)} - T*L_2^{(0)} + P(L_1^{(2)} + P*L_2^{(2)})] = 0 \qquad (3.5.b)$$

<u>Diamond – Liquid equilibrium line:</u>

$$\Delta G_C^{D/L}(X,T,P) = \Delta^0 H_C^{D/L} - T\Delta^0 S_C^{D/L} + P(K_1^{(3)} + PK_2^{(3)}) + RT \ln X_C^L + (1-X_C^L)^2[L_1^{(0)} - T*L_2^{(0)}) + P(L_1^{(3)} + P*L_2^{(3)})] = 0 \qquad (3.5.c)$$

where:
Me: Ni, Co:
$X_{Me}^{L} + X_{C}^{L} = 1$;
$\Delta^0 V_{Co}^{fcc/L}$ = constant;
$\Delta^0 V_{C}^{G/L} = [K_1^{(2)} + PK_2^{(2)}]$;
$\Delta^0 V_{C}^{D/L} = [K_1^{(3)} + PK_2^{(3)}]$;
$L^{(i)}_1$ $L^{(i)}_2$ = interaction parameters for free energy in liquid phase; i = 0, 1 ,2, 3;
$K^{(2)}_1$; $K^{(3)}_1$; $K^{(2)}_2$; $K^{(3)}_2$ = constant

While for C-Ni system at high pressure some experimental data is available, experimental data for C-Co system at high pressure is practically nonexistent.

To verify that mathematical relations developed for binary C-Me systems with eutectic at high pressure correctly describe solid-liquid (S-L) equilibrium lines, calculations were first made for carbon-nickel (C-Ni) system based on mathematical relations 3.5.a, 3.5.b, and 3.5.c. Calculated data were then compared with published experimental data.
Interaction parameters $L_1^{(0)}$ and $L_2^{(0)}$ are determined at P = 0 for two known experimental points (X, T) either from f.c.c. + L/L equilibrium line or from G+L/L equilibrium line, under the condition that the respective equation be verified simultaneously by both pair values (X, T).
High pressure experimental data regarding solubility of carbon (as graphite or diamond) in molten metal, as well as regarding melting of pure components (metal, graphite, diamond) is limited. In addition, experimental errors associated to melting points at high pressure (especially for graphite and diamond) are significant. Hence, interaction parameters $L_1^{(i)}$ and $L_2^{(i)}$ are determined separately for each equilibrium line under the condition that respective equations simultaneously verify two pairs of values (X, P, T).

Even less rigorous from the physical point of view, this approach allows to differently adjust the excess free energy term of C-Me solution for each equation, such that respective equations can be simultaneously verified by reciprocal experimental points, and by individual experimental points belonging to each equilibrium line, not only at moderate pressures but also at very high pressures.

Consequently, according to proposed mathematical model, the equilibrium phase diagram of a binary C-Me system with eutectic, is described by relations 3.5.a; 3.5.b; 3.5.c.
If $L_2^{(0)} = L_1^{(i)} = L_2^{(i)} = 0$, these relations describe solid/liquid equilibrium according to regular solution model.

3.1 Thermodynamic calculations

Calculation of C-Ni phase diagram at high pressure

Thermodynamic data for S-L transformation of pure components C, Ni and Co, is presented in Tab. 3.1. Experimental data used for the calculation of interaction parameters L and constants K, is presented in Tab. 3.2.
Calculated L and K values for solid/liquid (S/L) equilibrium in C-Ni system are shown in table 3.3. Comparison between calculated data and experimental data available for C-Ni system at high pressure is exhibited in Tab. 3.4.

Based on the agreement between the result of theoretical calculations with experimental data, we concluded that the mathematical model proposed for the calculation of S/L equilibrium diagrams in C-Me binary systems with eutectic is correct.

Calculation of C-Co phase diagram at high pressure

Thermodynamic data for S-L transformation of Co is presented in Tab. 3.1, while experimental data used for the calculation of interaction parameters L and constants K, are presented in Tab. 3.5.
Thus, dependence of temperature and concentration of Co-G eutectic and Co-D eutectic with pressure is described by following mathematical relations:

$$T_{EG} = 1548 + 11.3488 * P + 0.3682 * P^2 \quad (3.1.1)$$
$$X_{EG} = 11.6 + 0.5973* P + 0.0452 * P^2 \quad (3.1.2)$$

$$T_{ED} = 1453 + 22.1352 * P + 1.5071 * P^2 \quad (3.1.3)$$
$$X_{ED} = 15.5 + 0.4617 * P + 0.0688 * P^2 \quad (3.1.4)$$

Calculation of *"experimental points"* Co-G eutectic and Co-D eutectic was based on the assumption that their dependence of temperature and concentration is similar to that of Ni-G eutectic and Ni-D eutectic, for which experimental data at high pressure is available.

Temperature and concentration values of the points considered as *"experimental points"* in our calculations were calculated based on relations 3.1.1 to 3.1.4 and are displayed in Tab. 3.5.

The values of interaction parameters L and constants K were determined based on thermodynamic values for solid-liquid transformation of pure components in C-Co system, from table 3.1, and *"experimental data"* from Tab. 3.5. Calculated L and K values for solid/liquid (S/L) equilibrium in C-Co system are shown in Tab. 3.6.
Solid/liquid equilibrium phase diagrams of C-Co system computed based on the mathematical model developed, at 0 GPa; 5.01 GPa (pressure corresponding to invariant equilibrium Co^{fcc}/graphite/diamond/liquid); 5.6 GPa; 8.0 GPa and 12.5 GPa, are exhibited in Fig. 3.1. to 3.3.

Taking into account temperature and concentration data for G-L and D-L, resulted from calculation of solid-liquid equilibrium at different pressures, the following mathematical relations are obtained for pressure dependence of temperature and concentration for graphite/diamond equilibrium:

$$T_{GD} = 152.4 + 270.4331 * P + 4.1144 * P^2 \quad (3.1.5)$$

$$X_{GD} = 9.03 – 1.2685 * P + 0.5109 * P^2 \quad (3.1.6)$$

Graphic representation of dependence with pressure of temperature and concentration for cobalt-graphite eutectic and cobalt-diamond eutectic (described by mathematical relations 3.1.1 to 3.1.4), as well as of temperature and concentration of graphite/diamond/liquid equilibrium (described by mathematical relations 3.1.5 and 3.1.6), are presented in Fig. 3.4 and Fig. 3.5.
As it can be observed from Fig. 3.4, conditions for thermodynamic stability of diamond in C-Co system, are represented by pressure-temperature pair values included between melting line of diamond-cobalt eutectic line and graphite/diamond/liquid equilibrium line

It is worth mentioning that, using a pressure dependent asymmetrical model, Munke (33) calculated the phase diagram of C-Co at high pressure. However, as in the case of calculations by Peters and Dickinson, temperatures associated to graphite-cobalt eutectic, diamond-cobalt eutectic, and graphite/diamond/liquid equilibrium register unjustified increases with pressure.

Analyzing the solid/liquid equilibrium diagrams calculated at different pressures, the following conclusions regarding thermodynamic stability of diamond, that is, pressure-temperature conditions required for catalytic transformation of graphite to diamond in C-Co system can be drawn:

- *Pressure-temperature minimum conditions (P_0, T_0) required for diamond synthesis, are determined by the invariant equilibrium between all four phases present in the system: f.c.c.-Co/graphite/diamond/liquid; P_0 = 5.01 GPa; T_0 = 1601.5 K;*
- *For any given pressure value $P > P_0$ minimum and maximum temperature values for diamond synthesis are represented by temperature values pertaining to diamond-cobalt eutectic and, respectively, to graphite/diamond/liquid equilibrium, corresponding to that particular pressure;*
- *For any temperature value $T > T_0$ the minimum pressure for diamond synthesis is represented by pressure value pertaining to graphite/diamond/liquid, corresponding to that particular temperature.*

3.2 Kinetic calculations

It must be mentioned that experimental data regarding kinetics of HP-HT catalytic transformation of graphite to diamond, in C-Ni and C-Co systems is scarce.

Calculation of nucleation rate of diamond

According to this mechanism for catalytic transformation of graphite to diamond, diamond nuclei are formed as a result of statistical phase fluctuations that take place in carbon-metal solution, based on solid-solid transformation – homogeneous nucleation. Larger nuclei that survive phase fluctuations, become sites for diamond crystals growth.

To calculate the nucleation rate of diamond as a function of pressure and temperature, the following approximative relation was developed:

$$NR \sim \exp \{- C_1 / T [P - (a + bT)]^2\} \qquad (3.2.1)$$

where:
$C_1 = 16\pi\sigma^3 / 3\rho_D^2 (\Delta V)^2 K$ = constant
ρ is the diamond density;
σ is the superficial tension on the interface;
a and b are the constants of the graphite/diamond equilibrium line, with a = 0.6865 GPa and b = 0.00265 GPa/K, according to relation 3.1.

Since relation 3.2.1 has physical significance only for temperatures above melting temperature of metal in the presence of carbon, but below graphite/diamond equilibrium temperature, the nucleation rate is described by the following relation:

$$NR = C_0 \exp \{- C_1 / (T-T_E) * [P_{GD} – a – b (T_{GD} – T)]^2\} \qquad (3.2.2)$$

where:
T_E is the carbon-metal eutectic temperature;
P_{GD} and T_{GD} are pressure and temperature corresponding to graphite/diamond equilibrium.

The limiting pressure-temperature conditions for thermodynamic stability of diamond are derived from analysis of solid/liquid equilibrium diagrams, calculated at different pressures.
Thus, the approximate relationship 3.2.2. that described the rate of diamond nucleation as a function of pressure and temperature within the diamond thermodynamic stability domain was written as follows:

$$NR = C_0 \exp \{- C_1 / [(T_{GD} - \Delta T) - T_{ED}] * [P_{GD} + \Delta P - a - b(T_{GD} - \Delta T)]^2\} \qquad (3.2.3)$$

where:
T_{ED} is the diamond-cobalt eutectic temperature corresponding to graphite/diamond equilibrium pressure P_{GD};
T_{GD} is the diamond/graphite/liquid equilibrium temperature corresponding to graphite/diamond equilibrium pressure P_{GD};
P_{GD} is the pressure along isotherm T_{GD}; $P_{GD} \geq P_0$

a and b are the constants of the graphite/diamond equilibrium line, with a = 0.6865 GPa and b = 0.00265 GPa/K, according to relation 3.1.

Following substitutions were made in relation (3.2.3)
$T = (T_{GD} - \Delta T)$, is the temperature along isobar P_{GD} and is confined between T_{ED} and T_{GD};
$P = (P_{GD} + \Delta P)$, is the pressure along isotherm T_{GD} with $P_{GD} > P_0$

By analyzing the mathematical relation 3.2.3, which describes the dependence of nucleation rate with respect to pressure-temperature conditions from within the diamond thermodynamic stability domain, following considerations can be made:

- *For $P = P_0$ and $T = T_0$, implicitly $\Delta P = 0$ ($P_{GD} = P_0$) and $\Delta T = 0$ ($T_{GD} = T_0$), nucleation rate is zero, which means that under pressure-temperature conditions pertaining to invariant equilibrium: f.c.c.-Co/graphite/diamond/liquid, probability for diamond nuclei to form is zero;*
- *For $P = P_{GD} > P_0$, implicitly $\Delta P = 0$, nucleation rate along isobar P_{GD} is zero for $\Delta T = 0$ ($T = T_{GD}$), and is different from zero for $0 < \Delta T < T_{GD} - T_{ED}$ ($T_{ED} < T < T_{GD}$), which indicates that along isobar P_{GD}, probability of diamond nuclei to form, is zero for temperature corresponding to carbon-cobalt eutectic and, respectively for temperature corresponding to graphite/diamond/liquid equilibrium, and is different from zero for temperatures between these limits;*
- *For $T = T_{GD} > T_0$, implicitly $\Delta T = 0$, nucleation rate along isotherm T_{GD} is zero for $\Delta P = 0$ ($P = P_{GD}$) and increases for $\Delta P > 0$ ($P > P_{GD}$), which indicates that along isotherm T_{GD}, the probability for diamond nuclei to form is zero for temperature corresponding to graphite/diamond/liquid equilibrium, and increases for higher temperatures.*

The results of theoretical calculations for diamond nucleation rate as a function of pressure and temperature, are represented graphically in Fig. 3.6 and Fig. 3.7.
To conclude, dependence of nucleation rate with pressure and temperature conditions from within diamond thermodynamic stability domain, is described as follows:

- *At constant pressure, $P > P_0$, diamond nucleation rate is zero for the temperature corresponding to diamond-cobalt eutectic, rises rapidly to a maximum value for a temperature $T_{max} = (T_{GD} + 2T_{ED})/2$, and decreases slowly to zero for the temperature corresponding to graphite/diamond/liquid equilibrium;*
- *At constant temperature, $T > T_0$, diamond nucleation rate is zero for the pressure corresponding to graphite/diamond/liquid equilibrium, and increases with pressure, as long as the temperature does not exceed the diamond-cobalt eutectic temperature for any pressure value.*

Calculation of growth rate of diamond

In case of crystallization from solution, diffusion mechanism takes place as a result of existence of a crystallization film around nuclei in which concentration around saturation (X_0), is lower than concentration of supersaturated solution (X).
Concentration gradient ensures a diffusion flux so that, according to Fick law, crystal growth rate can be expressed as:

$$dm/dt = \beta S(X-X_0) \quad (3.2.4)$$

where:
dm/dt is the quantity of substance deposited on crystal surface in unit time;
β is the mass transfer coefficient;
S is the surface of growing crystal;
$X – X_0$ expresses supersaturation of solution.

Since β is determined by ratio of diffusion coefficient, D, and thickness of diffusion film, d, the above expression becomes:

$$dm/dt = D/d \ast S \ (\text{grad } X) \quad (3.2.5)$$

where:
grad $X = (X – X_0)$ is the concentration gradient.

If a spherical shape is assumed for diamond crystals, growth rate can be expressed as:

$$GR = dr/dt = 1/\rho * [D(X-X_0)/d] \quad (3.2.6)$$

where:
r is diamond crystal radius;
ρ is the diamond density;
D is diffusion coefficient;
X_0 is the concentration on crystal surface;
X is the concentration in supersaturated solution.

Assuming that at constant temperature, diffusion coefficient is constant and independent of concentration, within concentration range ($X-X_0$), and taking into account the thickness of 0.01 mm of metal catalyst film around the diamond crystal (27), relation (3.2.6), becomes:

$$GR = C (X – X_0) \quad (3.2.7)$$

where:
$C = D/\rho d$

Taking into consideration that $(X - X_0)$ represents the concentration difference between carbon concentration in carbon-metal solution, in graphite phase and diamond phase, at pressure-temperature conditions within diamond thermodynamic stability domain, the growth rate of diamond crystals was calculated using the following approximate relation:

$$GR = C\,(X_G^L - X_D^L) \qquad (3.2.8)$$

From analysis of solid/liquid equilibrium diagrams calculated for different pressures, it becomes clear that concentration difference between graphite and diamond in carbon-metal solution is dependent of thermodynamic parameters pressure-temperature.

The results of mathematical calculations regarding dependence of growth rate of diamond crystals with temperature at different pressures and with pressure at different temperatures are presented in Fig. 3.8 and Fig. 3.9. From these graphs, following conclusions can be drawn:

- *At constant pressure, $P > P_0$, diamond growth rate registers a maximum value for a temperature close to diamond-cobalt eutectic temperature and decreases with temperature increase, becoming zero for the temperature corresponding to graphite/diamond/liquid equilibrium, for which: $X_G^L = X_D^L$;*
- *At constant temperature $T > T_0$, diamond growth rate is zero for the pressure corresponding graphite/diamond/liquid equilibrium and increases with pressure increase, provided that temperature is higher than diamond-cobalt eutectic temperature, for any pressure value.*

Finally, based on the mathematical model developed for the HP-HT catalytic transformation of graphite to diamond (thermodynamic and kinetic calculations), the diamond synthesis process in binary carbon-metal systems with eutectic, subjected at pressures and temperate within the diamond thermodynamic stability domain, can be described as follows:

- *At pressure-temperature conditions in the vicinity of diamond-metal eutectic line, both nucleation rate and growth rate are high. Due to high nucleation and growth rates, under these conditions, a large number of low quality diamond crystals with high level of crystal growth defects (CGD) and residual metal catalyst (RMC) impurities can be synthesized. Diamond crystals will exhibit low mechanical strength;*

- *At pressure-temperature conditions away from diamond-metal eutectic line and graphite/diamond/liquid equilibrium line, nucleation rate and growth rate are lower. Due to reduced nucleation and growth rates, under these conditions, a lower number of medium quality diamond crystals with lower level of crystal growth defects (CGD) and residual metal catalyst (RMC) impurities can be synthesized. Diamond crystals will exhibit medium mechanical strength;*

- *At pressure-temperature conditions in the vicinity of graphite/diamond/liquid equilibrium line, both nucleation rate and growth rate are much lower. Due to much lower nucleation*

and growth rates, under these conditions, a small number of high-quality diamond crystals with low level of crystal growth defects (CGD) and residual metal catalyst (RMC) impurities, can be synthesized. Near graphite/diamond/liquid equilibrium line, large size, high-quality diamond crystals with high mechanical strength can be grown with time;

- *At pressures much higher than pressure corresponding to graphite/diamond/liquid equilibrium for any given temperature, nucleation and growth rates are very high. As a result, under these conditions, intergrown, twined (macles) and multicrystalline diamond crystals can be synthesized;*

- *At pressure-temperature conditions close to invariant equilibrium f.c.c.-metal/graphite/diamond/liquid, diamond synthesis conditions are uncertain. Thus, small pressure-temperature fluctuations will "remove" the system from diamond thermodynamic domain. Under these conditions, diamond crystals (if any) will be heavily included with graphite and metal.*

4. Experimental

High pressure apparatus

The opposed anvils high pressure apparatus, known as Bridgman anvils, is considered as ideal for high pressure generation, due to its simplicity and unlimited stroke, which allows unlimited compression of the pressure media. In its original design, the main disadvantage of Bridgman anvils apparatus is represented by the small volume of the sample subjected to compression, which makes this device unsuitable for diamond synthesis studies.

For the purpose of the study of HP-HT synthesis of diamond in carbon-cobalt system, a modified opposed anvils high pressure apparatus was design and built (34).
High pressure apparatus *"opposed anvils with spherical cavity"* employed in diamond synthesis experiments is shown schematically in Fig 4.1. a. and b.
In this design, the high pressure chamber of high pressure apparatus is enclosed between the spherical segment shaped depressions on top faces of the anvils. The total surface of the high pressure chamber is 16 cm^2. When fully compressed, high pressure chamber volume is approx. 4.0 cm^3, down from 5.0 cm^3, in uncompressed stage.
Sealing of the high pressure chamber was realized in two stages, using a combination of two gaskets: inner gasket, made of pyrophyllite, supported by an outer gasket made from polyamide resin. In compressed state, the gasket covers almost entirely the front faces of the anvils, so that high pressure generated inside the high pressure chamber, decreases gradually to atmospheric pressure, at the outer diameter of anvils. Consequently, the pressure gradient inside the reaction chamber is considerably reduced.

Diamond synthesis capsules

Diamond synthesis experiments were carried out using two types of diamond synthesis capsules: a) direct heating capsule and b) indirect heating capsule. Drawings of both types of diamond synthesis capsules are shown in Fig 4.2.

Pressure calibration at room temperature

Pressure calibration of the assembly comprised of high pressure apparatus and diamond synthesis capsule was performed using the so-called fixed pressure points technique. Pressure generated inside diamond synthesis capsule was measure by detecting the abrupt change in electrical resistivity, which accompanies the phase transitions of bismuth (Bi), thallium (Tl) and barium (Ba) with pressure.
Pressure values recommended for fixed pressure points on the international practical pressure scale are presented in Tab. 4.1.
Experimental setup for pressure calibration of both direct heating (a) and indirect heating (b) diamond synthesis capsules is shown in fig 4.3.
A number of five experiments were performed for the detection of each pressure point, and average value and variance of compressive force required for pressure generation, was calculated.
In Tab. 4.2, experimental data acquired in pressure calibration experiments are presented as pressure at transition points vs. press force. Data on pressure generation efficiency (E) at pressure points and relative error (I) in pressure generation, calculated according to relations (4.1) and (4.2) respectively, is also included in Tab. 4.2.

$$E = S*P / 2F \quad (4.1)$$

$$I = s / F \quad (4.2)$$

where:
S is the total surface of high pressure chamber;
P is the pressure generated inside the capsule;
F is the compressive force (press force) used to generate pressure P;
s is the average squared deviation (variance) calculated for compressive force.

Pressure calibration curves for direct heating capsule (a) and indirect heating capsule (b) described by mathematical relations (4.3) and (4.4), for pressures between 2.0 GPa and 8.0 GPa, are presented in Fig. 4.4.

a) $P = 0.0995 + 0.659 F + 0.0208 F^2$ (4.3)

b) $P = 0.3751 + 1.029 F + 0.0249 F^2$ (4.3)

Temperature calibration at high pressure

Temperature inside diamond synthesis capsules was measured at 5.5 GPa, with the aid of Ni/CrNi thermocouple.
Experimental setup for pressure calibration of both direct heating (a) and indirect heating (b) diamond synthesis capsules is shown in Fig. 4.5.
A number of five temperature measurements were performed for each data point, and average value and standard deviation of temperature generated inside the capsule, for the same level of electrical power, were calculated.
Temperature values were corrected for pressure effect on thermocouple.
Temperature calibration curves for direct heating capsule (a) and indirect heating capsule (b) described by mathematical relations (4.4) and (4.5), for temperature range between 25^{o}C and 1600 ^{o}C are presented in Fig. 4.6

a) $T = 22 + 1242\ W + 4.8\ W^2$ (4.4)

b) $T = 25 + 1429\ F - 155.3\ W^2$ (4.5)

Confirmation of pressure and temperature calibration of high pressure apparatus and capsule

The techniques of pressure calibration using fixed pressure points and temperature calibration with thermocouple are unanimously accepted and practiced by those involved in high pressure research.
Pressure-temperature calibration of the high pressure apparatus-capsule assembly was verified by comparing our calibration results with experimental results obtained by others.
For this purpose, *alpha iron* (αFe) – gamma iron (γFe) equilibrium line was determined experimentally for pressures up to 8.0 GPa.
It is known that at normal pressure and temperatures up to 1183 K, *alpha* phase of iron with volume centered cube (v.c.c.) structure is the stable phase. At temperatures above 1183 K, *gamma* phase of iron with face centered cube (f.c.c.) structure becomes the stable phase.
In order to detect the αFe – γFe transition, the capsule for diamond synthesis was assembled as shown in Fig. 4.7. The capsule so assembled made possible temperature measurement with the aid of Ni/CrNi thermocouple, simultaneously with measurement of the electrical resistance of an iron wire.
Transition a*lpha* - *gamma* (on heating) and *gamma* - a*lpha* (on cooling) are accompanied by significant variations of the electrical resistance of the iron wire. The resistance vs. temperature graph acquired at 7.0 GPa is presented in Fig. 4.8. As it can be seen from Fig. 4.8, temperature corresponding to αFe – γFe transition at this pressure is 562 ^{o}C and the transition interval is 65^{o}C.
In Tab. 4.3, our experimental data is presented together with experimental data obtained by Clougherty and Kaufman (36).
Based on the data acquired in the calibration experiments, we concluded that experimental errors in evaluation of pressure and temperature conditions associated with diamond synthesis experiments are approx. ± 0.1 GPa and ± 20^{o}C.

5. **Experimental study of diamond synthesis in carbon-cobalt system**

The experimental study of diamond synthesis in carbon-cobalt system consisted of experiments designed to ascertain the pressure-temperature conditions for diamond synthesis and the nucleation and growth rates of diamond, as a function of pressure and temperature.

High pressure phase quenching technique was used in all diamond synthesis experiments.
Practically, phase quenching under high pressure was accomplished based on the algorithm, depicted in Fig 5.1:

- Pressure was increased to a pre-established value and maintained constant for a set time interval;
- Following a set time (needed for high pressure uniformization) temperature was increased to a pre-established value and was maintained constant for a set time interval (reaction time);
- Once reaction time expired, temperature was reduced rapidly under existing high pressure;
- Following a set time (needed for quenching the phases formed under high pressure), the pressure was reduced to atmospheric pressure.

High pressure phase quenching experiments to determine pressure-temperature parameters for diamond formation were performed under the following pressure-temperature-time conditions: P = 5.2 GPa – 6.0 GPa; T = 1300 ^{o}C to 1700 ^{o}C; t = 60 sec.

Diamond nucleation and growth experiments were performed at constant pressure, P = 5.6 GPa, and variable temperature, T = 1300 ^{o}C - 1550 ^{o}C, and at constant temperature, T = 1475 ^{o}C, and variable pressure, P = 5.2 GPa – 6.2 GPa, respectively. In all diamond nucleation and growth experiments the reaction time was set for 300 sec.

Following extraction from capsule, graphite-cobalt specimens reacted under different pressure-temperature-time conditions, were inspected under optical microscope, for visual detection of diamond crystals, and then chemically processed for removal of unreacted graphite and cobalt.
Presence or absence of diamond was the only criteria used to evaluate the results of high pressure quenching experiments, designed to determine pressure-temperature conditions for diamond formation. Experimental results for diamond formation in the carbon-cobalt system are presented in Tab. 5.1 and displayed graphically in Fig. 5.2. Based on these experimental results, diamond synthesis in carbon-cobalt system takes place under pressure-temperature conditions comprised between line 1, which represents the high temperature limit and line 2, which represents the low temperature limit. The intersection of these two lines defines the minimum pressure-temperature conditions for diamond system: 5.0 GPa < P_0 < 5.2 GPa; 1325 < T_0 < 1350.
In Tab. 5.2, pressure-temperature conditions for thermodynamic stability of diamond in carbon-cobalt system at P = 5.6 GPa, calculated using the mathematical model developed, are compared with pressure-temperature conditions for diamond formation in carbon-cobalt system obtained in our diamond synthesis experiments at P = 5.6 GPa.

Recovered diamond crystals from nucleation and growth experiments were first weighted and then analyzed for particle size distribution. Subsequently, optical microscopy, scanning electron microscopy and inductively couple plasma spectroscopy analysis were performed to assess the quality of synthesized diamond crystals.

Optical microscopy and scanning electron microscopy images of synthesized diamond crystals, present in carbon-cobalt reaction charge extracted from diamond capsule following a diamond synthesis cycle, are presented in Fig. 5.3.

Diamond nucleation rate was calculated according to the following formula:

$$NR = N / V * t \quad (5.1)$$

Using experimental data, the number of crystals was calculated for each diamond nucleation experiment according to the following approximate relation:

$$N = \sum_{k=1}^{n} p_k * n_k \quad (5.2)$$

where:
p_k is the mass of crystals of size k in carats;
n_k is the approximate number of crystals of size k in unit mass (one carat).

The approximate number of particles per carat and the average diameter of diamond crystals per size grade used in these calculations is depicted in Tab. 5.3.
Experimental conditions and the number of diamond crystals calculated according to (5.2) are included in Tab. 5.4.
Since in all these experiments, graphite volume subjected to HP-HT treatment and reaction time were kept constant, V_G = 0.4 cm^3, t = 300 sec., the number of diamond crystals is directly proportional with nucleation rate.

Graphic representation of nucleation rate as a function of temperature at constant pressure and, as a function of pressure at constant temperature, was obtained by fitting the data calculated for the number of crystals, for each pressure-temperature pair value, from Tab. 5.3, using the following mathematical relations:

$$N(T) = C_1 \exp [- C_2 / (T - T_m) (T_M - T)^2] \quad (5.3)$$

$$N(P) = C_3 \exp [- C_4 / (P - P_m)^2] \quad (5.4)$$

For P = 5.6 GPa, numerical values of constants C_1 and C_2 together with T_m (low temperature limit) and T_M (high temperature limit) values, are listed below:

N (T) (nr. crystals)	NR (T) (nr. crystals/ cm^3 *s)
$C_1 = 3.334 * 10^6$	$C'_1 = 0.027 * 10^6\ cm^{-3}\ s^{-1}$
$C_2 = 0.632 * 10\ ^oC^{-3}$	
$T_m = 1325\ ^oC$	
$T_M = 1550\ ^oC$	

For T = 1475 ^oC, numerical values of constants C_3 and C_4 together with P_m (low pressure limit) and P_M (high pressure limit) values, are listed below:

N (P) (nr. crystals)	NR (P) (nr. crystals/ cm^3 *s)
$C_3 = 4.338 * 10^6$	$C'_3 = 0.036 * 10^6\ cm^{-3}\ s^{-1}$
$C_4 = 0.546 * 10\ GPa^{-2}$	
$P_m = 5.4\ GPa$	

Dependence of nucleation rate with temperature at constant pressure, and with pressure at constant temperature is displayed in Fig. 5.4.a and b., respectively.

Crystal growth rate, expressed as linear growth of diamond crystal diameter per unit time, was calculated as follows:

$$GR = \Delta d_{avg} / \Delta t \qquad (5.5)$$

Using the data presented in Tab. 5.3, the average size (diameter) of crystals was calculated, according to following approximate relationship:

$$d_{avg} = \sum_{k=1}^{n} p_k * d_k = \frac{1}{2} \sum_{k=1}^{n} p_k * (d_k + d_{k-1}) \qquad (5.6)$$

where:
d_k, d_{k-1} represent maximum and minimum diameter of crystals belonging to class size k;
n_k is the approximate number of crystals of size k in unit mass (one carat).

Experimental conditions and the growth rate of diamond crystals calculated according to (5.6) are included in Tab. 5.5.

For a set time interval, growth rate is directly proportional to the linear growth of the average diameter of diamond crystals. It is worth mentioning that, in the case of diamond synthesis experiments performed at constant pressure, due to thermal inertia of diamond capsule, the effective reaction (synthesis) time is not rigorously constant and depends on temperature. Therefore, to avoid experimental errors that could be introduced by thermal inertia of the capsule, in our crystal growth calculations, reaction time was measured from the moment the graphite-cobalt specimen started to melt, which was detected by abrupt change of electrical

resistance of the specimen. Therefore, as presented in Tab. 5.5 reaction time shorter at lower temperatures and reaches the set value at higher temperatures.
Similarly, graphic representation of growth rate as a function of temperature at constant pressure and as a function of pressure at constant temperature, was achieved by fitting data calculated for the average size of diamond crystals, for each pressure-temperature pair value shown in Tab. 5.4, using the following mathematical relations:

$$GR(T) = K_1 + K_2 * T + K_3 T^2 \quad (5.7)$$

$$GR(P) = K_4 + K_5 * P + K_6 P^2 \quad (5.8)$$

For P = 5.6 GPa, numerical values of K_1, K_2 and K_3, are listed below:

d_{avg} (T) (μm)	GR (T) (μm/s)
K_1 = -234.84 μm	K'_1 = -234.84 μm s^{-1}
K_2 = 71.7 * 10^{-2} μm $^oC^{-1}$	K'_2 = 71.7 * 10^{-2} μm $^oC^{-1}$ s^{-1}
K_3 = -31.2 * 10^{-5} μm $^oC^{-2}$	K'_3 = -0.104 * 10^{-5} μm $^oC^{-2}$ s^{-1}

For T = 1475 ^{o}C, numerical values of K_4, K_5 and K_6, are listed below:

d_{avg} (T) (μm)	GR (T) (μm/s)
K_4 = 119.36 μm	K'_4 = 2.336 μm s^{-1}
K_5 = -3.02 μm GPa^{-1}	K'_5 = -0.672 μm s^{-1} GPa^{-1}
K_6 = 1.01 μm GPa^{-2}	K'_6 = 0.0625 μm s^{-1} GPa^{-2}

Dependence of growth rate with temperature at constant pressure and with pressure at constant temperature is displayed in Fig. 5.5.a. and b.

By analyzing the graphs presented in Fig. 5.4.a and b representing the dependence of nucleation rate with temperature at constant pressure and with pressure and constant temperature, we concluded as follows:

- *At constant pressure, with temperature increase, the nucleation rate (number of diamond crystals) increases at maximum value, then decreases slowly to zero following an asymmetric curve;*
- *At constant temperature, with pressure increase, the nucleation rate (number of diamond crystals) increases continuously.*

Similarly, analysis of the graphs presented in Fig. 5.5.a and b, representing the dependence of growth rate with temperature at constant pressure, and with pressure and constant temperature, indicates that:

- *Under constant pressure and set time, growth rate (average size of diamond crystals) decreases with temperature increase;*
- *Under constant temperature and set time, growth rate (average size of diamond crystals) increases with temperature increase.*

Crystallographic phase analysis of graphite-cobalt specimens reacted under HP-HT conditions

In an attempt to understand metal catalyst contribution to graphite-diamond transformation, X-ray diffraction analysis was performed on graphite-cobalt specimens reacted to different - pressure-temperature conditions. In addition, X-ray diffraction analysis was performed on material resulted after reacted graphite-cobalt specimens were chemically (dissolution of cobalt in diluted nitric acid) and physically (separation of diamond from graphite in bromoform) processed.
Experimental conditions and the results of phase analysis by X-ray diffraction are included in Tab. 5.6. X-ray diffraction data reveal that diamond, as new phase, was detected in graphite-cobalt specimens reacted at pressure-temperature conditions at which diamond is thermodynamically stable (i.e. P =5.6 GPa; T = 1450 ^{o}C). On the other hand, if the graphite-cobalt specimen was reacted under pressure-temperature conditions at which diamond is not thermodynamically stable (i.e. P = 4.8 GPa; T = 1350 ^{o}C), only the initial phases, graphite and cobalt, were detected.
Following cobalt removal and diamond separation from graphite-cobalt specimens reacted under same pressure-temperature conditions, X-ray diffraction shows that untransformed carbon remains in initial phase – graphite.

To conclude, the results of phase analysis clearly indicate that following the treatment of graphite-cobalt catalyst specimens, at high pressure and high temperature, the only structural transformation is graphite-diamond transformation. No other phases and/or intermediary compounds, as precursors to graphite-diamond transformation, were identified.

6. Characterization of physical and chemical properties of synthesized diamond crystals

Nature and content of metallic impurities in synthesized diamond crystals

Analysis of the nature and content of impurities in diamond crystals synthesized under different pressure-temperature conditions was done by X-ray diffraction and inductively coupled plasma (ICP) spectroscopy. For this scope, diamond crystals of size 120/140 mesh (average size of approx. 115 μm) were chosen. Nature and concentration of residual cobalt impurities of diamond crystals synthesized under different pressure-temperature conditions are presented in Tab. 6.1. Cobalt content in diamond crystals synthesized at 5.6 GPa and temperatures ranging from 1375 ^{o}C to 1525^{o}C is graphically displayed in Fig. 6.1.
As mentioned above, due to thermal inertia of the diamond synthesis capsule, in Tab. 6.1, reaction time has lower values at lower temperatures, and reaches the set value at higher temperatures.
Since only spectroscopic purity graphite and cobalt were used in all high pressure-high temperature experiments, synthesized diamond crystals contain only cobalt as metallic impurity

in detectable concentrations. Data represented in Tab. 6.1, show clearly that cobalt is present in diamond crystals in f.c.c. phase; high temperature *beta* phase of cobalt. This result is in accordance with experimental results obtained by Wong (37). Using extended X-ray absorption fine structure (EXAFS) technique, coupled with conventional transmission electron microscopy (TEM), X-ray diffraction and X-ray fluorescence techniques, Wang confirmed that metallic impurities Ni, Co, Fe are present as f.c.c. crystallographic phases in the crystalline structure of diamond. Furthermore, using X-ray diffraction and metallographic techniques to analyze basic structural characteristics of phases presented as impurities in diamond crystals synthesized in carbon-nickel and carbon-cobalt systems, Vavrda (38), concluded that these impurities are not carbides, but primary solid solutions of carbon in the metal catalyst.
Data presented in Tab. 6.1 and Fig. 6.2 a. and b, also show a strong correlation between cobalt concentration in diamond crystals synthesized at different pressure-temperature conditions, specifically:

- *At constant pressure, P = 5.6 GPa, concentration of cobalt impurities decreases with temperature;*
- *At constant temperature, T = 1475 ^{o}C, concentration of cobalt impurities increases with pressure.*

Morpho-structural characteristics of synthesized diamond crystals

Due to pressure and temperature gradients inside the capsule, synthesized diamond crystals do not share same particle size and crystal characteristics (morphology, topography, crystal growth defects, color and transparency, etc.).
To study the morpho-structural characteristics of synthesized diamond the following pressure-temperature-time conditions were used: P = 5.2 GPa – 6.2 GPa; T = 1375 ^{o}C - 1525 ^{o}C, t = 600 sec. Taking into consideration that diamond crystals sharing same size range do not share same physical characteristics, such as crystal morphology (growth habit), surface topography (roughness) and color and transparency, the morpho-structural characterization of synthesized diamond crystals was made by defining the following main crystal types:

- Type A: crystals with cubic morphology featuring well developed (100) faces, heavily included, gray to black colors, opaque crystals;
- Type B: crystals with cubic morphology featuring well developed (100) faces and less developed (111) faces, deep yellow to light yellow colors, translucent and transparent crystals;
- Type C: crystals with cub-octahedron morphology featuring well developed (111) faces and less developed (100) faces, light yellow color, transparent crystals;
- Type D: crystals with no identifiable morphology, irregularly shaped, yellowish gray to gray colors, translucent crystals.

Since, in a sample of diamond crystals two or more types of diamond crystals and even atypically diamond crystals are present, in our analysis we singled out the predominant crystal type (highest weight percentage crystals). The results of morpho-structural analysis of diamond crystals synthesized under different pressure-temperature conditions are presented in Tab. 6.2.

Dependence of morpho-structural characteristics of diamond crystals with pressure and temperature can be summarized as follows:

- *At constant pressure with temperature increase, crystal growth habit evolves from predominantly cube with well developed (100) faces – type A crystals – to predominantly cub-octahedron with well developed (100) faces and less developed (111) faces – type B crystals – to predominantly cub-octahedron with well developed (111) faces and less developed (100) faces – type C crystals;*
- *At constant temperature with pressure increase, crystal growth habit evolves from predominantly cube with well developed (100) faces – type A crystals – to predominantly cub-octahedron with well developed (100) faces and less developed (111) faces – type B crystals – to predominantly crystals with no identifiable morphology, exceedingly irregularly shaped crystal – type D crystals.*

Mechanical strength of synthesized diamond crystals

Mechanical strength is controlled by intrinsic properties of diamond crystals. To a great extent, size, morphology, concentration of crystal growth defects (CGD) and residual metal catalyst (RMC) impurities are responsible for mechanical strength of diamond crystals.
Mechanical strength of diamond crystals was determined based on "on size" toughness test technique; toughness index being calculated as follows:

$$TI = (M / M_t) * 100 \ (\%) \qquad (6.1)$$

Toughness index was determined on diamond crystals of 50/60 mesh size or 250 - 297 μm (average size of approx. 274 μm), synthesized under different pressure-temperature conditions.
Toughness index of diamond crystals synthesized at constant pressure and different temperatures is included in Tab. 6.3 and graphically displayed in Fig. 6.3.
Toughness index of diamond crystals synthesized at constant temperature and different pressures is included in Tab. 6.4 and graphically displayed in Fig. 6.4.

Toughness index data indicate a strong dependence of mechanical strength of diamond crystals with pressure-temperature synthesis conditions, as follows:

- *At constant pressure, mechanical strength of diamond crystals increases with temperature;*
- *At constant temperature, mechanical strength of diamond crystals decreases with pressure.*

7. Conclusions

- *A theoretical approach to catalytic diamond synthesis, by way of a mathematical model, has been proposed with the purpose of understanding the mechanism of the catalytic transformation of graphite to diamond in the binary Carbon-Metal (C-Me) systems with eutectic, at high pressure and high temperature (HP-HT);*

- *The mathematical model developed provides a representation of the HP-HT catalytic transformation of graphite to diamond in binary carbon-metal systems with eutectic from both thermodynamic and kinetic standpoint;*

- *The mathematical model developed, describes reasonably accurate the process of high pressure-high temperature catalytic transformation of graphite to diamond in binary carbon-metal systems with eutectic and has been reasonably validated, by comparing calculated data with from literature available for nickel-carbon system, and with experimental data acquired through diamond synthesis experiments in carbon-cobalt system, as follows:*
    - *calculated vs. experimental data from literature for carbon-nickel system at different pressures: 0 GPa, 2.6 GPa, 5.2 GPa, 5.4 GPa and 6.0 GPa, presented in Tab. 3.4;*
    - *calculated vs. experimental minimum and maximum temperatures required for diamond synthesis at P = 5.6 GPa presented in Tab. 5.2;*
    - *nucleation rate of diamond calculated as a function of temperature, at constant pressure, presented in Fig. 3.6, with experimental data acquired for dependence of nucleation rate of diamond with temperature, at constant pressure, presented in Tab. 5.4 and Fig. 5.4.a;*
    - *nucleation rate of diamond calculated as a function of pressure, at constant temperature, presented in Fig. 3.7, with experimental data acquired for dependence of nucleation rate of diamond with pressure, at constant temperature, presented in Tab. 5.4 and Fig. 5.4.b;*
    - *growth rate of diamond calculated as a function of temperature, at constant pressure, presented in Fig. 3.8, with experimental data acquired for dependence of growth rate of diamond with temperature, at constant pressure, presented in Tab. 5.5 and Fig. 5.5.a;*
    - *growth rate of diamond calculated as a function of pressure, at constant temperature, presented in Fig. 3.9, with experimental data acquired for dependence of growth rate of diamond with pressure, at constant temperature presented in Tab. 5.5 and Fig. 5.5.b.*

- *For a given graphite-metal catalyst system and under pressure-temperature conditions for which diamond is thermodynamically stable, intrinsic properties of diamond crystals are determined by nucleation and growth rates, which are controlled via pressure-temperature process parameters, thus:*
    - *subject to low nucleation and growth rates, well developed (cuboctahedron), large size diamond crystals with low level of crystal growth defects (CGD), residual metal catalyst (RMC) impurities and high mechanical strength could be synthesized;*
    - *subject to high nucleation and growth rates, poorly developed (irregular shaped), small size diamond crystals with high level of crystal growth defects (CGD), residual metal catalyst (RMC) impurities and low mechanical strength could be synthesized*

- *Understanding the mechanism that governs the HP-HT catalytic transformation of graphite to diamond, represents a valuable approach toward an efficient control of the diamond synthesis processes, thus enabling synthesis of diamond crystals, whose physical and chemical properties are controlled by way of preassigned pressure-temperature synthesis parameters.*

References:

1. F. P. Bundy, J. Chem. Phys. 38(1980) 6930
2. F.P. Bundy, H.T, Hall, H.M. Strong, R.H. Wentorf, Nature 176 (1955), 51
3. H.P. Bovenkerk, F.P. Bundy, H.T. Hall, H.M. Strong, R.H. Wentorf, Nature 184 (1959) 1094
4. F.P. Bundy, H. P. Bovenkerk, H. M. Strong, R. H. Wentorf, J. Chem. Phys. 35 (1961) 383
5. A. A. Jardini, J. E. Tydings, S. B. Litvin, Am. Mineralogist 45 (1960) 27
6. H. Liander, E. Lundblad, Arkiv. Kemi. 16 (1960) 139
7. A. A. Jardini, J. E. Tydings, S. B. Litvin, Am. Mineralogist 47 (1962) 1393
8. R. H. Wentorf, H. P. Bovenkerk, J. Chem. Phys., 36 (1962) 1987
9. C. M. Higgins, P. Cannon, Nature, 194 (1962) 829
10. H. M. Strong, J. Chem. Phys., 39 (1963) 2057
11. L. F. Vereschaghin, et. al., Dokl. Akad. Nauk. 162 (1965) 1027
12. 47. M. Wakatsuki, Japan J. Appl. Phys., 5 (1966) 337
13. H. J. Rodewald, Chinia 15 (1961) 251
14. Yu. A. Litvin, Izv. Akad. Nauk. SSSR Neorg. Mat., 4 (1968) 175
15. P. Cannon, E.T. Collins, in “Reactivity of Solids” ed. G. H. Swab, Elsevier, Amsterdam 1965
16. R. H. Wentorf, Ber, Bunsenges. Phys. Chem. 70 (1966) 975
17. V. P. Butuzov et all., Rest Krist., 9 (1972) 69
18. L. F. Vereschaghin, et all., Dokl. Akad. Nauk. 192 (1970) 768
19. L. F. Vereschaghin, et all., Sovrem. Prob. Fiz. Kim. 1 (1968) 173
20. G. B. Bokii, A. I. Volkov, Kristalografiya 14 (no. 1) (1969)
21. A. A. Jukov, Jurnal Fiziceskoi Himii 41 (1967) 185
22. V. A. Ianciuk, Sverthverdie Materiali 5 (1980) 16
23. L.S. Palatnik, L. L. Gladkin, Dokl. Akad. Nauk SSSR (1971) 81
24. L.S. Palatnik, s.a. Fiz Tverd. Tela (1973) 2029
25. E.T. Peters, L. Kaufman, J.J. Ryan, “AFCRL Report 65 – 168”; Contract No. AF19 (628) 2466, february 1965
26. S. K. Dickinson, “AFCRL Report 70.0620”, Physical Research Papers No. 434, November 1970, Air Force Cambridge Research Laboratories, Bedford, MA., USA
27. H. M. Strong, R. E. Hanneman, J. Chem. Phys. Vol. 46 No 9 (1967) 3668
28. R. Berman, F. Simon, Z. Elekrokem. 59 (1955) 333
29. M. Hansen, K. Anderco, “Constitution of Binary Alloys” (Mc. Graw Hill, N.Y. 1958)
30. H. M. Strong, Acta Metalurgica, 12 (1964) 1411
31. F. P. Bundy, J. Geophys. Res. 85 (1980) 6930

32. R. Berman, Thermal Properties in “Physical Properties of Diamond” ed. R. Berman (Clarendon Press, Oxford, 1965)
33. G. Munke, Diamond Research (1974) 7
34. I. Benea et all., *“High pressure apparatus for the synthesis of superhard materials”* RO Patent Nr. 90871/1986
35. V. E. Bean, S. Akimoto, P. M. Bell, S. Block, W. B. Holtzapel, M. H. Manghani, M. F. Nicol, S. M. Stishov, in “Research in High Pressure Science and Technology”, Proc. Of 10th AIRAPT Conf. 1985, ed N. J. Trappeniers, et all. (North Holland, Amsterdam 1986) 52
36. E. V. Clougherty, L Kaufman, ASME Publication Paper No 62 – WA -258, 1963
37. J. Wong, E. F. Koch, C. I. Hejna, M.F. Garbausas, J. Appl. Phys., 58 (1985) 3388
38. T Vavrda, Sverhtverdie Materiali, 3 (1981) 27

Tables & Figures:

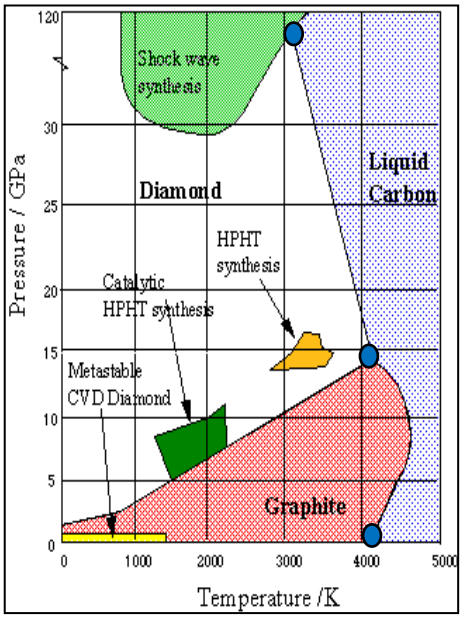

Diamond-Liquid equilibrium line:
diamond/metal/liquid triple point (hypothetic)
T ~ 2,800 K; P ~ 50 GPa
graphite/diamond/liquid triple point
T = 4,100 ± 100 K; P = 11 ± 1.0 GPa
Graphite-Liquid equilibrium line:
graphite/diamond/liquid triple point
P = 4,100 ± 100 K; P = 11 ± 1.0 Gpa
graphite/liquid/vapor triple point:
P = 4,020 ± 50 K; P = 0.011 – 0.014 GPa
max. point: T ~ 4,600 K; P ~ 6.5 GPa
Graphite-Diamond equilibrium line:
P (GPa) = 0.6865 + 0.00265 T (K) (Berman-Simon)
P (GPa) = 1.94 + 0.0025 T (°C) (Kennedy)

Fig. 1.1 Phase diagram of Carbon (Bundy 1980)

Tab. 3.1 – Thermodynamic data for S-L transformation of pure components C, Ni and Co

Transformation	DH (J/mol)	DS (J/mol*K)	DV (cm^3/mol)	Reference
G - L	90,376.50	-22.594	--	(25, 26)
D - L	89,121.30	-27.364	--	(25, 26)
Ni^{cfc} - L	17,614.60	-10.209	0.337	(25, 26)
Co^{cfc} - L	16,192.00	-9,163	0.263	(26)

Tab. 3.2 – Experimental data used for the calculation of interaction parameters L and constant K

System	Equilibrium line	Point	X*10^{-2} (at%)	T (K)	P(GPa)	Reference
Ni - C	G + L/ L	eutectic	0.088	1587	10^{-4}	(29)
		melting	0.200	2500	10^{-4}	(29)
		eutectic	0.137	1661	5.4	(27)
		eutectic	0.150	1600	6.7	(30)
	D + L / L	eutectic	0.135	1665	5.3	(29)
		eutectic	0.134	1667	5.4	(29)
C	G / L	melting	1.000	4000	6.5	(31)
		melting	1.000	4200	12.5	(31)
	D / L	melting	1.000	3350	6.5	(32)
		melting	1.000	4200	12.5	(31)

Tab. 3.3 – Calculated L and K values for solid/liquid equilibrium in C-Ni system

System	Equilibrium line	$E_G^L = X_{Me} * X_C((L_1^{(0)} - T*L_2^{(0)} + P(L_1^{(i)} + L_2^{(i)}))$				$V_C^{G,D/L} = K_1^{(i)} + P*K_2^{(i)}$	
		$L_1^{(0)}$ (J/mol)	$L_2^{(0)}$ (J/mol)	$L_1^{(i)}$ (J/mol)	$L_2^{(i)}$ (J/mol)	$K_1^{(i)}$ (cm^3/mol)	$K_2^{(i)}$ (cm^3/mol)
	Ni^{cfc} + L / L	-72721.35	-28.786	-1462.30	309.61	--	--
	(I = 1)						
Ni - C	G + L / L	-72721.35	-28.786	-8222.30	443.08	5.40	-0.4032
	(I = 2)						
	D + L / L	-72721.35	-28.786	-387.23	271.96	2.52	-0.0369
	(I = 3)						

Tab. 3.4 - Comparison between calculated data and experimental data available for C-Ni system at high pressure

Point	Calculated data			Experimental data			
	$X*10^{-2}$ (at%)	T (K)	P(GPa)	$X*10^{-2}$ (at%)	T (K)	P(GPa)	Reference
Ni-G	0.088	1586.4	10^{-4}	0.091-0.112	1580-1591	10^{-4}	(29)
eutectic	0.112	1621.0	2.6	0.110	1637	2.6	(27)
	0.137	1660.9	5.4	0.137	1661	5.4	(27)
	0.143	1669.6	6.0	0.144	1670	6.0	(30)
Ni-D							
eutectic	0.134	1666.1	5.4	0.134	1667	5.4	(27)
G/D/L							
equilibrium	0.143	1729.6	5.4	0.150	1728	5.4	(27)
Ni(cfc)/G/L							
equilibrium	0.135	1658.1	5.2	0.135	1665	5.25	(27)

Tab. 3.5 – Experimental data used for the calculation of interaction parameters L and constant K

System	Equilibrium line	Point	$X*10^{-2}$ (at%)	T (K)	P(GPa)	Reference
		eutectic	0.116	1547	10^{-4}	(29)
		melting	0.200	2250	10^{-4}	(29)
Co - C	G + L/ L	eutectic*	0.158	1616	5.4	calculated
		eutectic*	0.172	1636	6.7	by similarity
	D + L / L	eutectic*	0.159	1665	5.0	with Ni-C
		eutectic*	0.158	1667	5.4	system
	G / L	melting	1.000	4000	6.5	31
C		melting	1.000	4200	12.5	31
	D / L	melting	1.000	3350	6.5	32
		melting	1.000	4200	12.5	31

Tab. 3.6 – Calculated L and K values for solid/liquid equilibrium in C-Co system

System	Equilibrium line	$E_G^L = X_{Me} * X_C((L_1^{(0)} - T*L_2^{(0)} + P(L_1^{(i)} + L_2^{(i)}))$				$V_C^{G,D/L} = K_1^{(i)} + P*K_2^{(i)}$	
		$L_1^{(0)}$ (J/mol)	$L_2^{(0)}$ (J/mol)	$L_1^{(i)}$ (J/mol)	$L_2^{(i)}$ (J/mol)	$K_1^{(i)}$ (cm^3/mol)	$K_2^{(i)}$ (cm^3/mol)
	Co^{cfc} + L / L	69,870.75	-22.258	-1067.73	309.61	--	--
	(i = 1)						
Co - C	G + L / L	69,870.75	-22.258	-7929.51	443.08	5.40	-0.4032
	(i = 2)						
	D + L / L	69,870.75	-22.258	-3306.19	271.96	2.52	-0.0369
	(i = 3)						

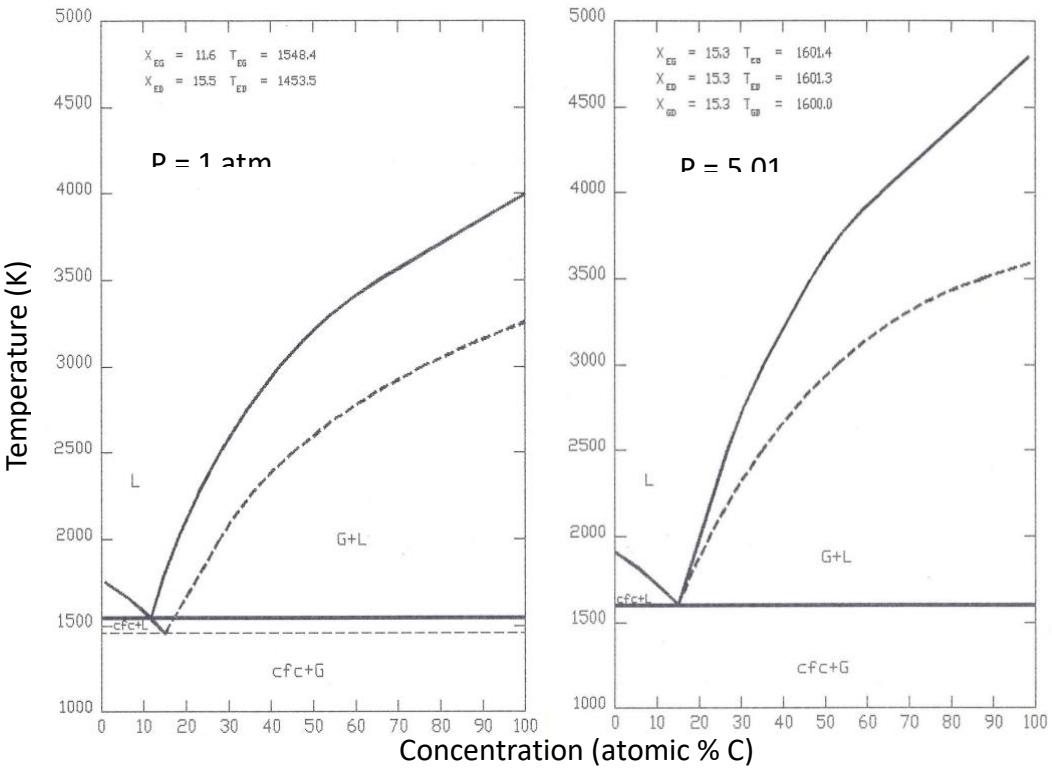

Fig. 3.1 – Solid/liquid equilibrium phase diagrams of C-Co system calculated at 1 atm and 5.01 GPa

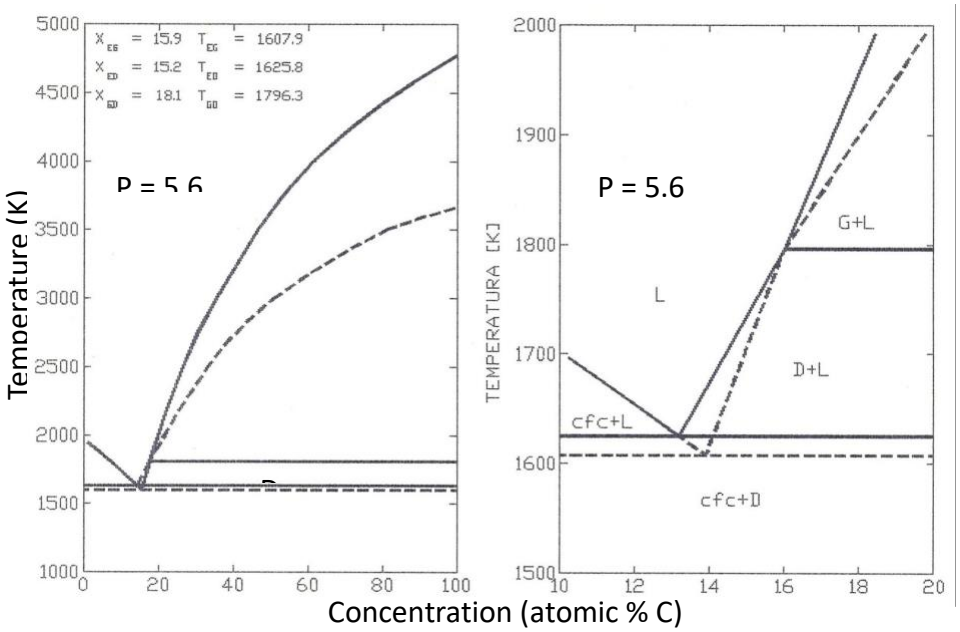

Fig. 3.2 – Solid/liquid equilibrium phase diagrams of C-Co system calculated at 5.6 GPa

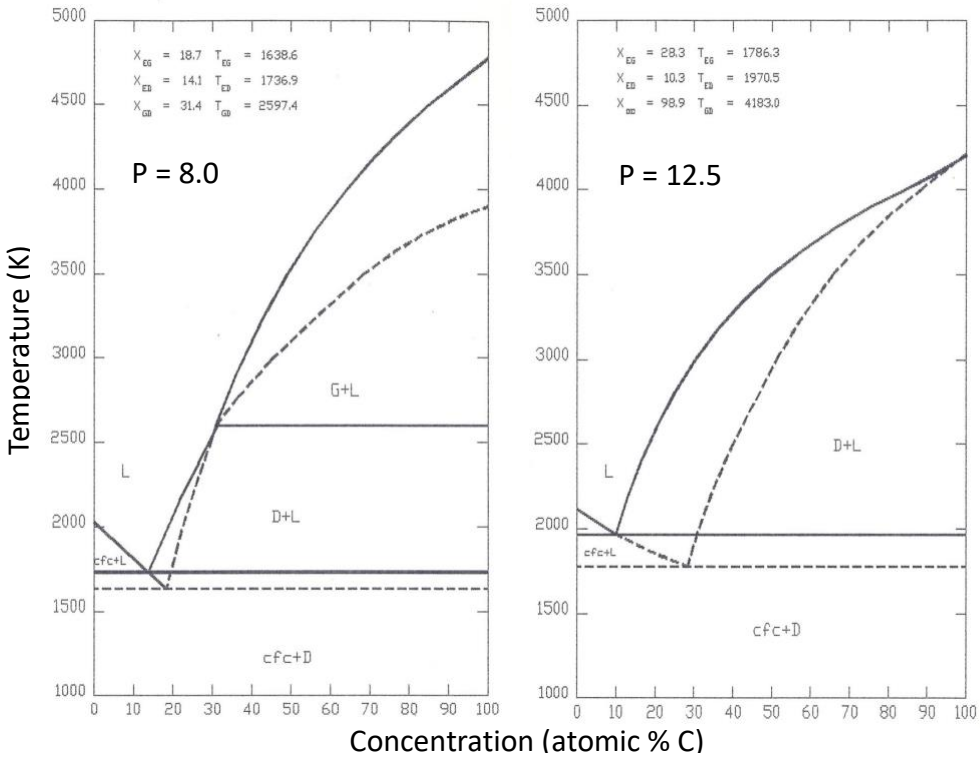

Fig. 3.3 – Solid/liquid equilibrium phase diagrams of C-Co system calculated at 8.0 GPa & 12.5 GPa

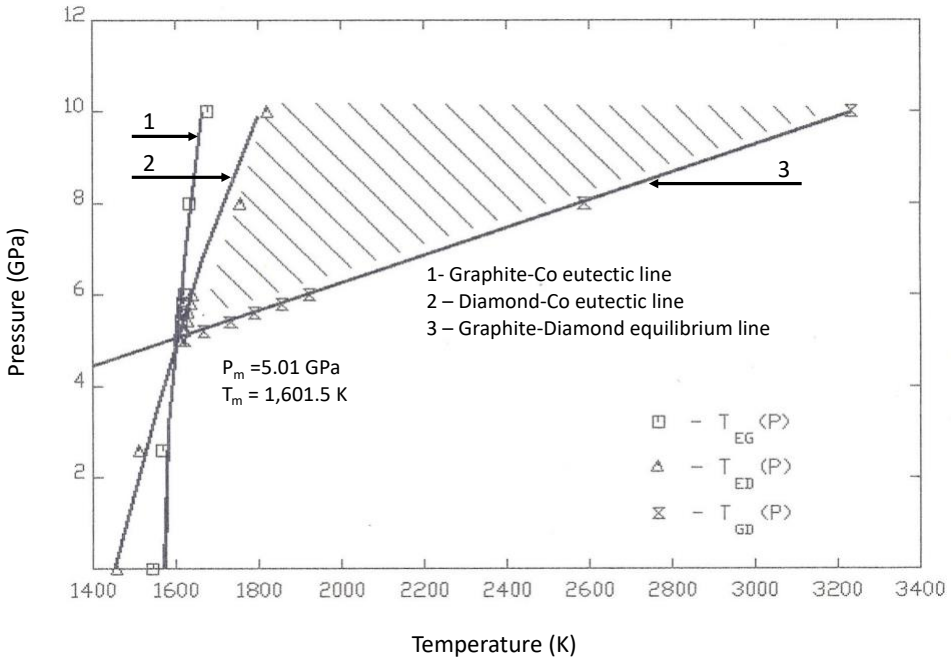

Fig. 3.4 – Pressure dependence of temperature of cobalt-graphite eutectic, cobalt-diamond eutectic and graphite/diamond/liquid equilibrium

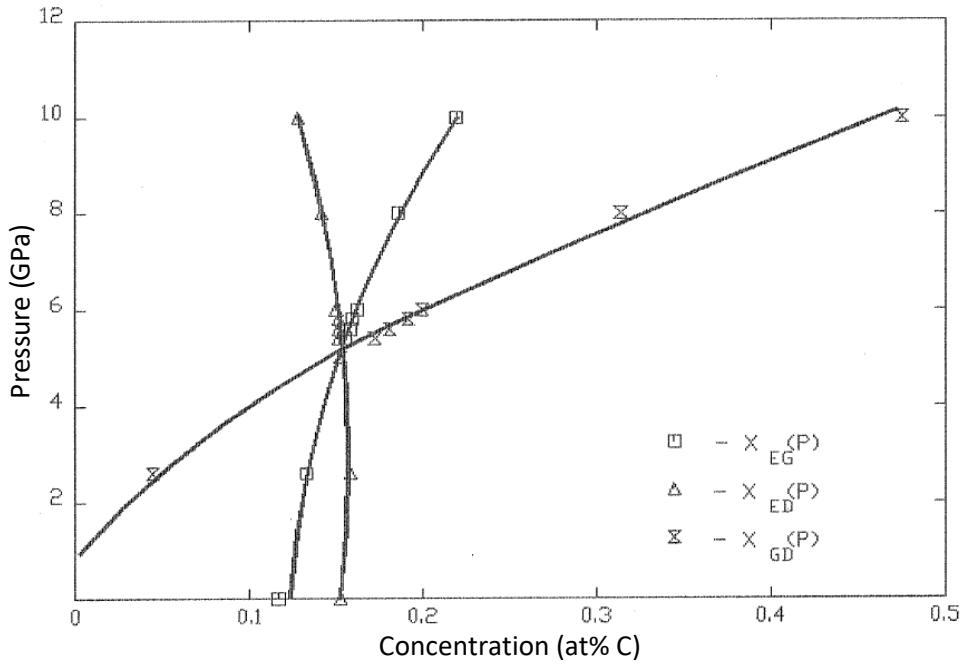

Fig. 3.5 – Dependence of carbon concentration with pressure for cobalt-graphite eutectic, cobalt-diamond eutectic and graphite/diamond/liquid equilibrium

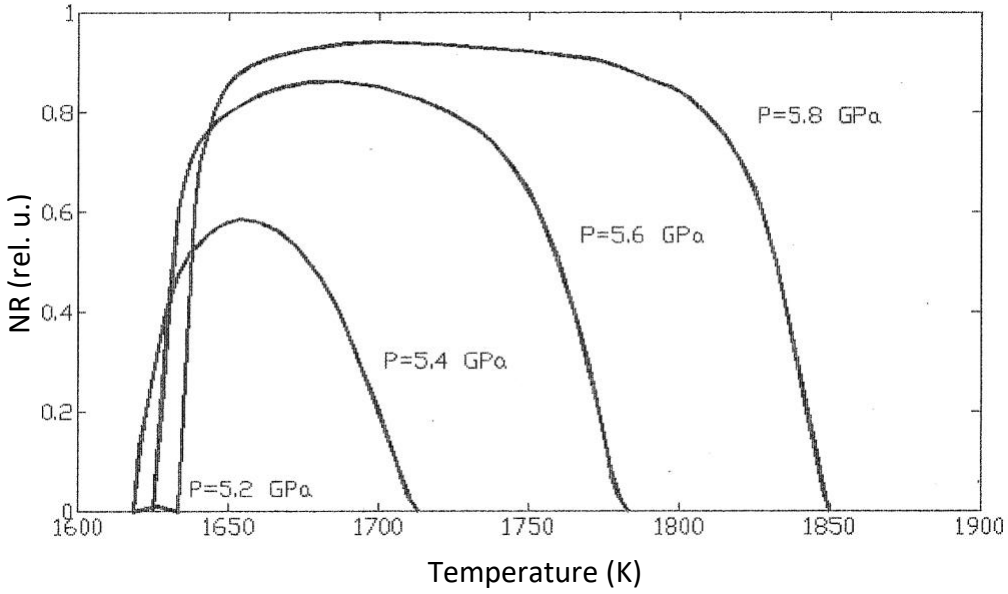

Fig. 3.6 – Dependence of nucleation rate of diamond with temperature at constant pressure

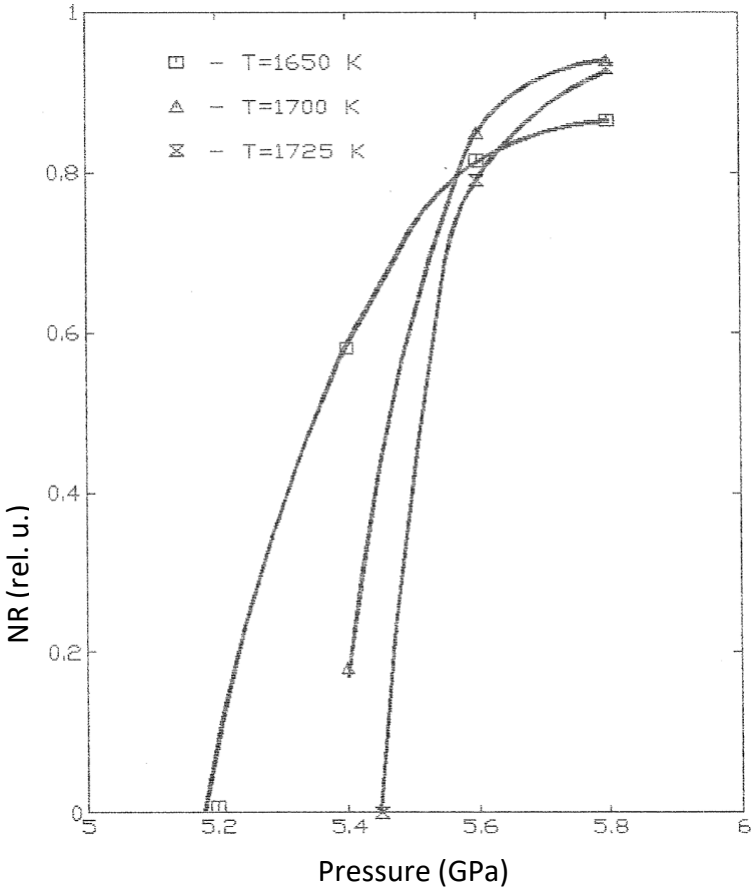

Fig. 3.7 – Dependence of nucleation rate of diamond with pressure at constant temperature

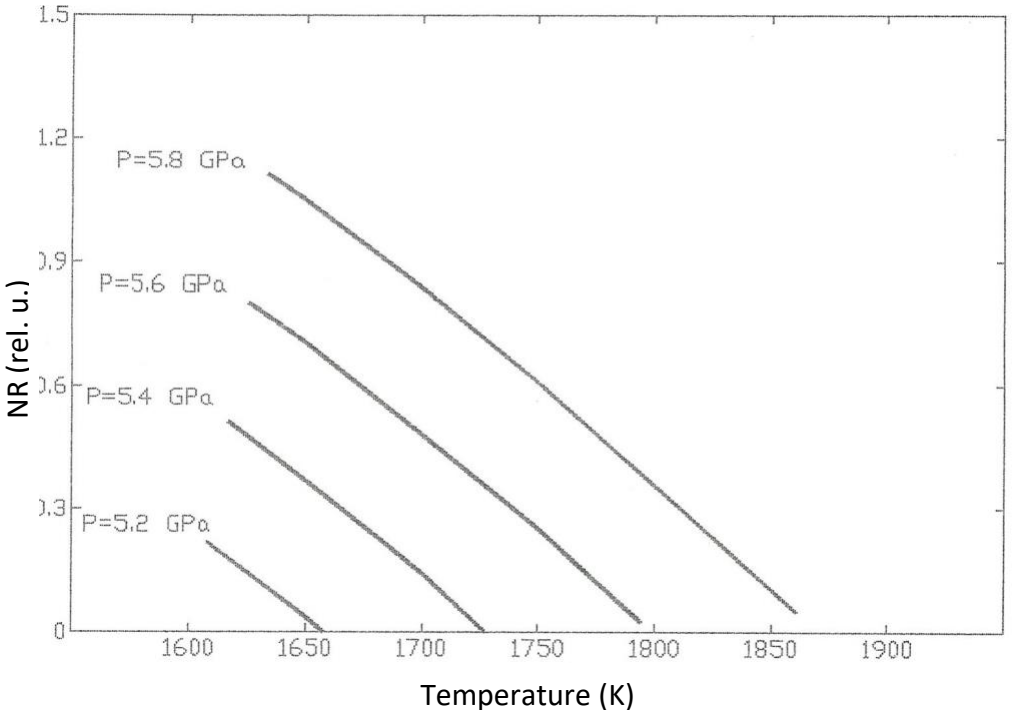

Fig. 3.8 – Dependence of growth rate of diamond with temperature at constant pressure

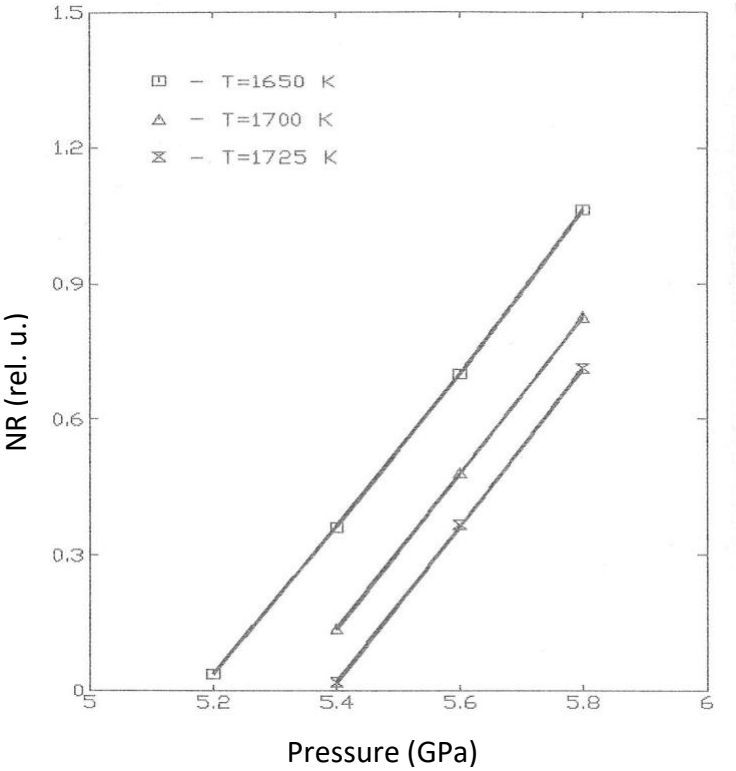

Fig. 3.9 – Dependence of growth rate of diamond with pressure at constant temperature

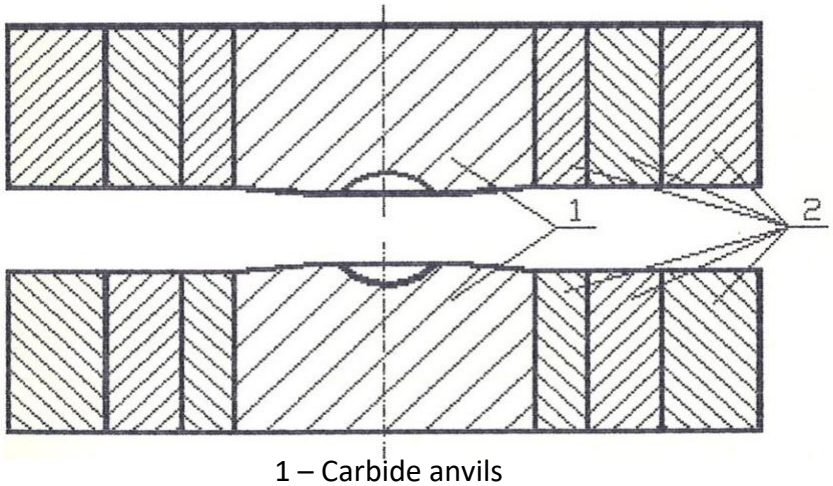

1 – Carbide anvils
2 – Steel rings

Fig. 4.1.a – High pressure apparatus assembly

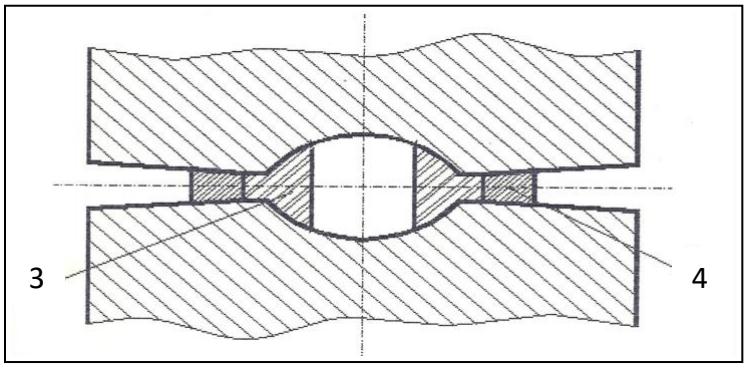

3 – Pyrophyllite gasket
4 – Resin gasket

Fig. 4.1.b – Gasket assembly

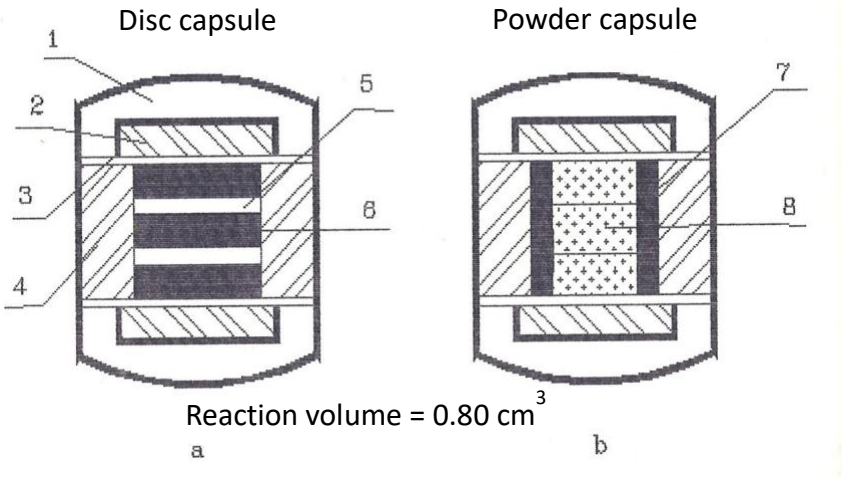

1 – Steel end cap
2 – Ceramic insulator
3 – Metal disc (Mo)
4 – Pyrophyllite disc
5 – Cobalt disc
6 – Graphite disc
7 – Graphite cylinder
8 – Graphite-Cobalt powder mix

Fig. 4.2 – Capsule assembly

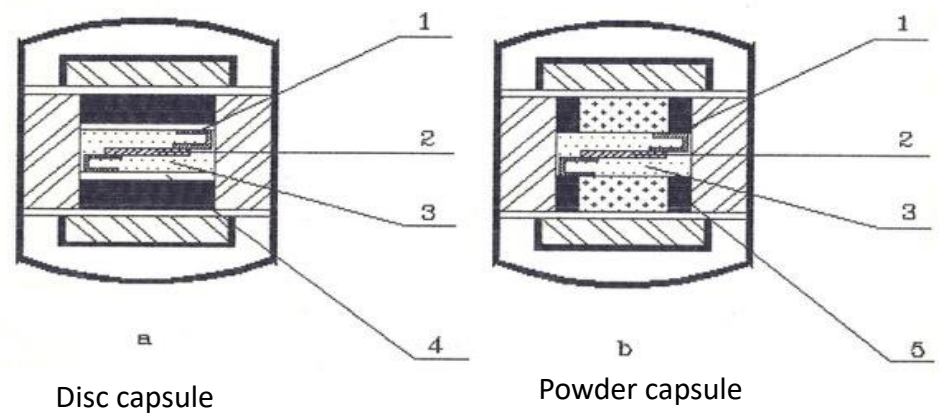

1 – Electric contact (Cu)
2 – Pressure sensor (Bi; Tl; Ba)
3 – NaCl media
4 – Metal disc (Mo)
5 - Graphite heater

Fig. 4.3 – Experimental setup for pressure calibration of both direct heating (a) and indirect heating (b)

Tab. 4.1 – Pressure values recommended for fixed pressure points on the international practical pressure scale

Pressure (GPa)	2.550 ± 0.006	3.68 ± 0.03	5.5 ± 0.1	7.7 ± 0.2	9.4 ± 0.3	12.3 ± 0.5	13.4 ± 0.6
Transition	Bi I-II	Tl II-III	Ba I-II	Bi III-V	Sn	high-Ba	Pb
Reference	(35)						

Tab. 4.2 – Experimental data acquired in pressure calibration experiments

		Direct heating capsule				Indirect heating capsule			
Transition	Pressure (GPa)	F (MN)	s (MN)	I (%)	E (%)	F (MN)	s (MN)	I (%)	E (%)
Bi I-II	2.55	2.21	0.04	1.8	92.3	2.18	0.04	1.8	93.5
Tl II-III	3.68	3.59	0.07	1.9	81.5	3.63	0.08	2.2	81.1
Ba I-II	5.50	5.67	0.13	2.2	76.4	5.64	0.14	2.4	78
Bi III-V	7.70	8.10	0.18	2.2	76.0	9.17	0.22	2.4	67.2

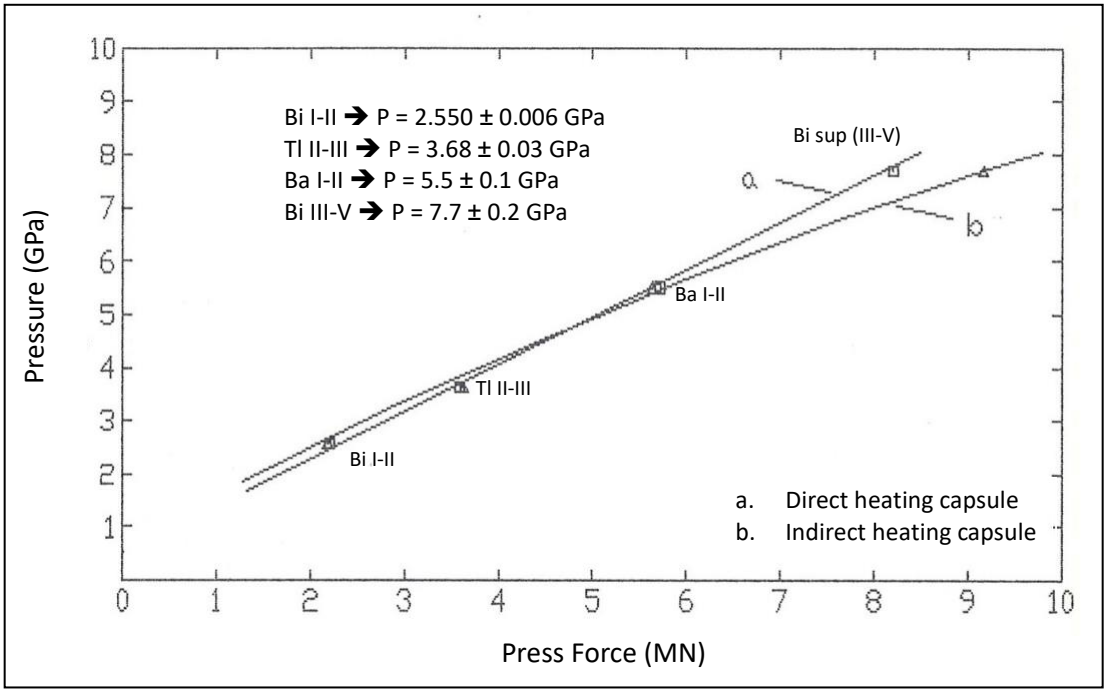

Fig. 4.4 – Pressure calibration curves for direct heating capsule (a) and indirect heating capsule

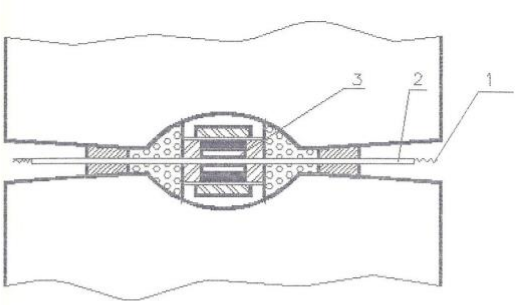

Disc capsule (direct heating)

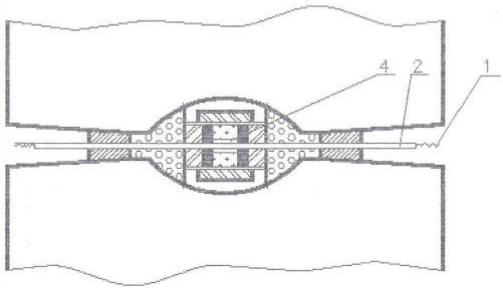

Powder capsule (indirect heating)

1 – Thermocouple Ni/CrNi (type K)
2 – Ceramic tube
3 – Graphite disc
4 – hBN disc

Fig. 4.5 – Experimental setup for temperature calibration of both direct heating (a) and indirect heating (b)

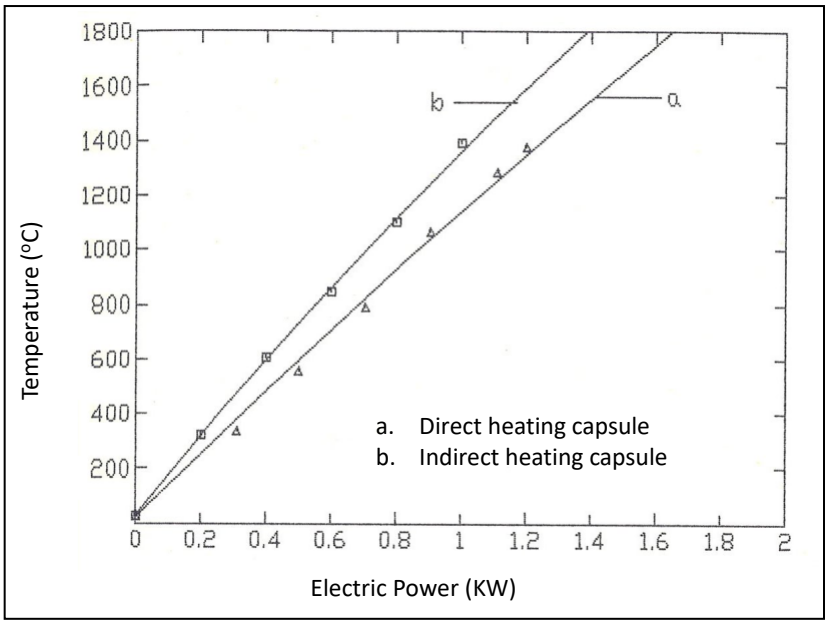

Fig. 4.6 – Temperature calibration curves for direct heating capsule (a) and indirect heating capsule

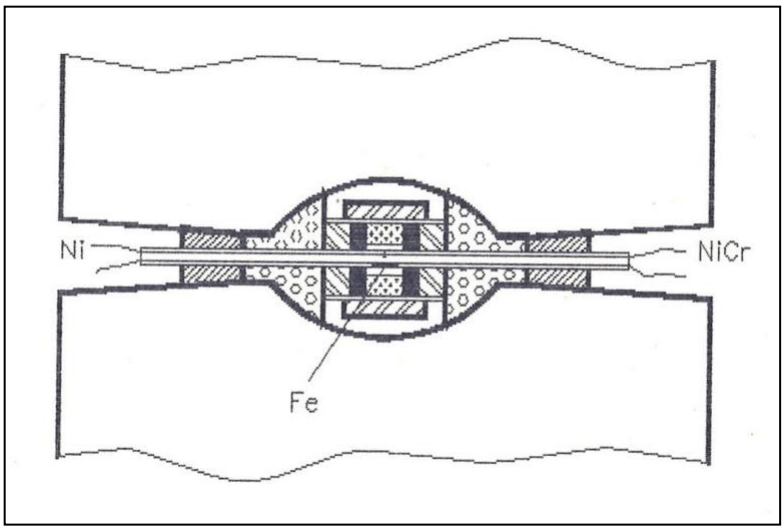

Fig. 4.7 – Experimental setup for detection of αFe – γFe transition at high pressure

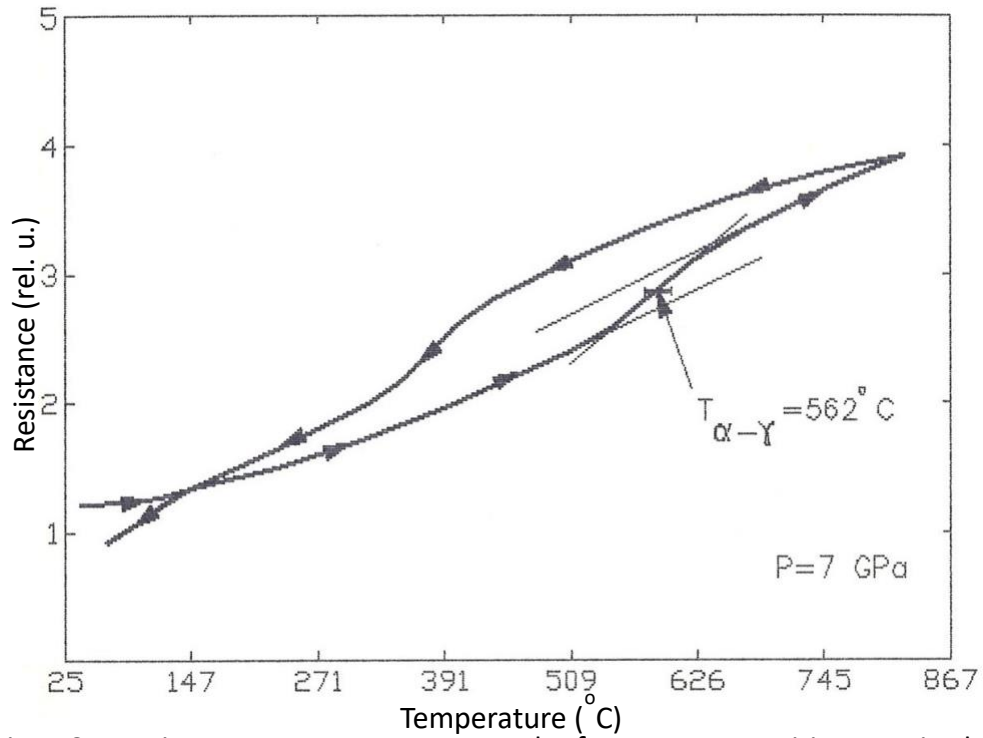

Fig. 4.8 – Resistance vs. temperature graph of αFe – γFe transition acquired at 7.0 GPa

Tab. 4.3 – Experimental data experimental vs. literature data (36) for αFe – γFe transition at high pressure

Fe^a ➔ Fe^g equilibrium (P,T)										
P(GPa)		0	2.5	3.5	3.6	5.5	7.0	7.5	7.7	0
T(oC)	This work	910	747	n.a.	702	632	**562**	n.a.	545	522
	Literature	910	735	705	n.a.	620	**575**	553	n.a.	540

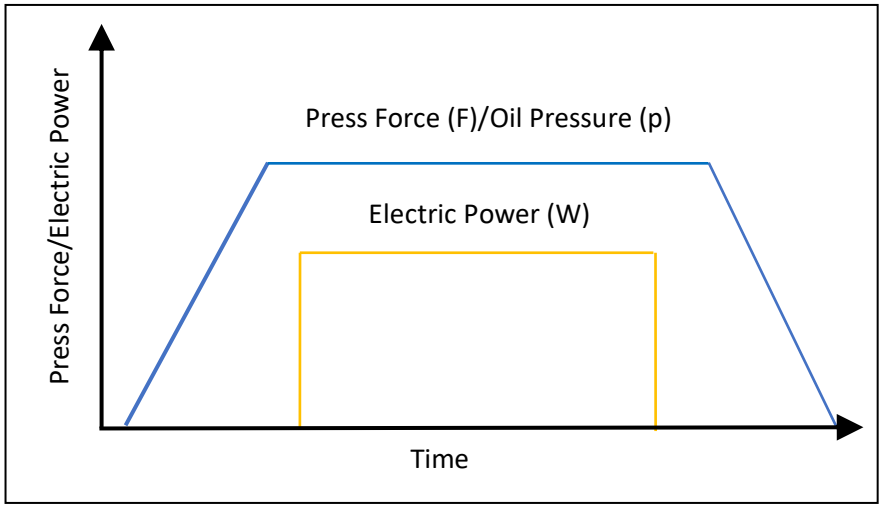

Fig. 5.1 – Press force-electric power-time diagram used for diamond synthesis experiments

Tab. 5.1 – Experimental results for diamond formation in the carbon-cobalt system

P (GPa)	6.0	6.0	6.0	6.0	6.0	6.0	6.0	6.0	6.0	6.0	6.0	6.0	6.0	6.0
T (oC)	1300	1325	1350	1375	1400	1425	1475	1525	1575	1625	1650	1575	1700	1725
D/no-D	o	o	o	●	●	●	●	●	●	●	●	●	o	o

P (GPa)	5.8	5.8	5.8	5.8	5.8	5.8	5.8	5.8	5.8	5.8		
T (oC)	1300	1325	1350	1375	1400	1450	1500	1550	1575	1600	1625	1650
D/no-D	o	o	o	●	●	●	●	●	●	●	o	o

P (GPa)	5.6	5.6	5.6	5.6	5.6	5.6	5.6	5.6	5.6	5.6
T (oC)	1300	1325	1350	1375	1400	1450	1500	1525	1550	1575
D/no-D	o	o	●	●	●	●	●	●	o	o

P (GPa)	5.4	5.4	5.4	5.4	5.4	5.4	5.4	5.4	5.4
T (oC)	1300	1325	1350	1375	1400	1425	1450	1475	1500
D/no-D	o	o	●	●	●	●	●	o	o

P (GPa)	5.2	5.2	5.2	5.2	5.2	5.2	5.2
T (oC)	1300	1325	1350	1375	1400	1425	1450
D/no-D	o	o	●	●	●	o	o

P (GPa)	5.0	5.0	5.0	5.0
T (oC)	1300	1325	1350	1375
D/no-D	o	o	o	o

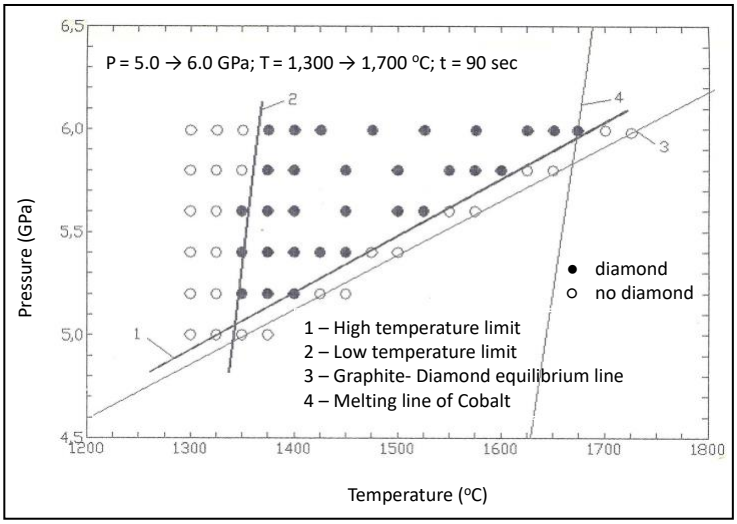

Fig. 5.2 – Graphic representation of pressure-temperature conditions for diamond synthesis in C-Co system

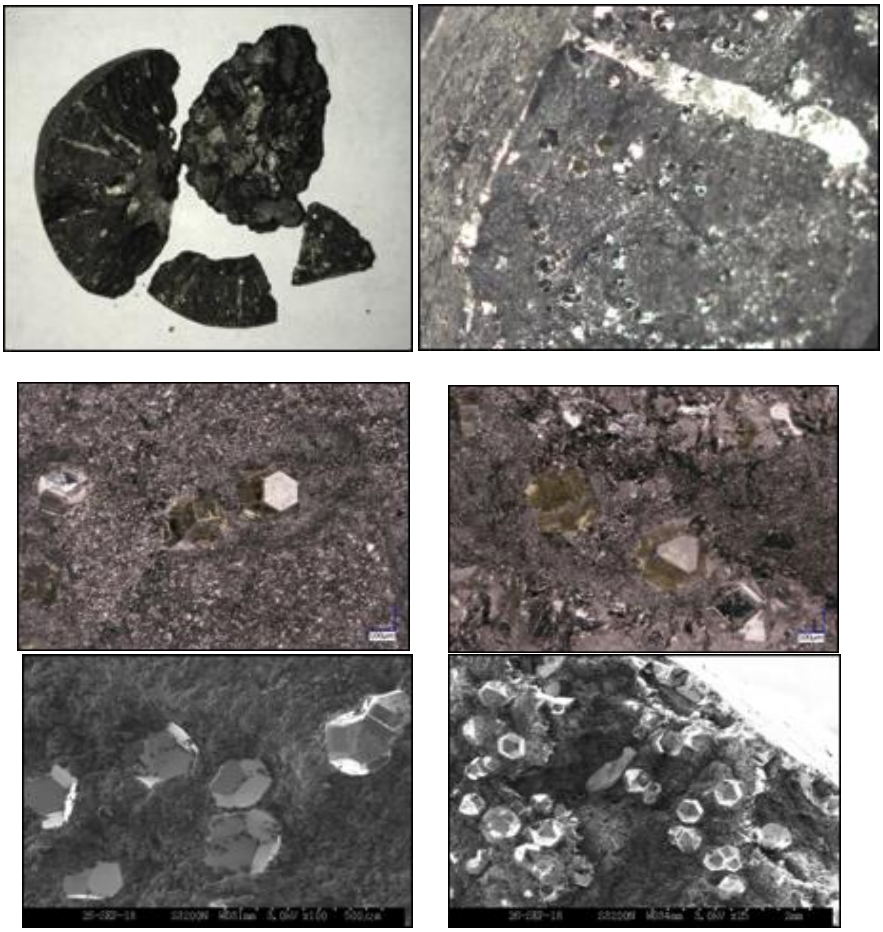

Fig. 5.3 – Optical and scanning electron microscopy images of synthesized diamond crystals

Tab. 5.2 – Experimental vs. calculated pressure-temperature conditions for diamond synthesis at P = 5.6 GPa

Experimental data (this work)			Calculated data (this work)		
P		T	T		
(GPa)		°C	°C	K	
P = 5.6	T_{min}	1350	1353	1626	T_{ED}
	T_{max}	1525	1523	1796	T_{GD}

Tab. 5.3 – Average particle diameter per size grade and approx. number of particles per carat

ANSI	FEPA	Sieve Opening	Avg. Diameter	Number
325/400	D46	44-37	40.5	1,130,000
270/325	D54	53-44	48.5	660,000
230/270	D64	63-53	58.0	384,000
200/230	D76	74-63	68.5	252,000
170/200	D91	88-74	81.0	140,000
140/170	D107	105-88	96.5	83,400
120/140	D126	125-105	115.0	49,400
100/120	D151	149-125	137.0	20,820
80/100	D181	177-149	163.0	17,140
60/80	D252	250-177	213.5	10,400
50/60	D301	297-250	273.5	3,240
40/50	D427	420-297	358.5	2,080

Tab. 5.4 – Experimental results and total number of particles (nucleation rate)

P	T	t	Md	Particle Size Distribution (ct)											N
(GPa)	(°C)	(sec)	(ct)	D252	D181	D151	D126	D107	D91	D76	D64	D54	D46	< D46	
5.6	**1325**	**300**	0												**0.00**
5.6	**1350**	**300**	11.9	2.2	2.2	1.9	1.6	1.1	1.0	0.5	0.5	0.3	0.3	0.3	**$1.95*10^6$**
5.6	**1375**	**300**	13.6	3.3	2.7	2.0	1.6	1.0	0.9	0.4	0.5	0.3	0.3	0.7	**$2.61*10^6$**
5.6	**1425**	**300**	13.9	3.4	2.9	2.5	0.9	1.4	1.1	0.4	0.4	0.3	0.3	0.3	**$1.98*10^6$**
5.6	**1475**	**300**	9.5	2.0	2.1	1.7	1.3	0.7	0.6	0.2	0.3	0.2	0.1	0.3	**$1.33*10^6$**
5.6	**1500**	**300**	7.3	1.7	1.7	1.4	1.0	0.5	0.4	0.1	0.2	0.1	0.1	0.2	**$0.80*10^6$**
5.6	**1525**	**300**	3.7	0.4	0.7	0.9	0.7	0.4	0.3	0.1	0.1	0.1	0.0	0.1	**$0.47*10^6$**
5.6	**1550**	**300**	0												**0.00**

P	T	t	Md	Particle Size Distribution (ct)											N
(GPa)	(°C)	(sec)	(ct)	D252	D181	D151	D126	D107	D91	D76	D64	D54	D46	< D46	
5.4	**1475**	**300**	0.0												**0.00**
5.6	**1475**	**300**	18.4	7.5	2.9	2.3	1.9	1.3	1.0	0.4	0.4	0.3	0.2	0.2	**$0.79*10^6$**
5.8	**1475**	**300**	27.1	12.3	3.9	3.0	2.6	1.7	1.6	0.6	0.6	0.4	0.2	0.3	**$2.21*10^6$**
6.0	**1475**	**300**	31.7	12.7	4.5	3.7	3.2	2.1	2.1	0.8	0.9	0.6	0.5	0.7	**$3.80*10^6$**
6.2	**1475**	**300**	36.7	12.5	5.8	4.6	4.1	2.8	2.7	1.1	1.2	0.8	0.6	0.7	**$4.46*10^6$**

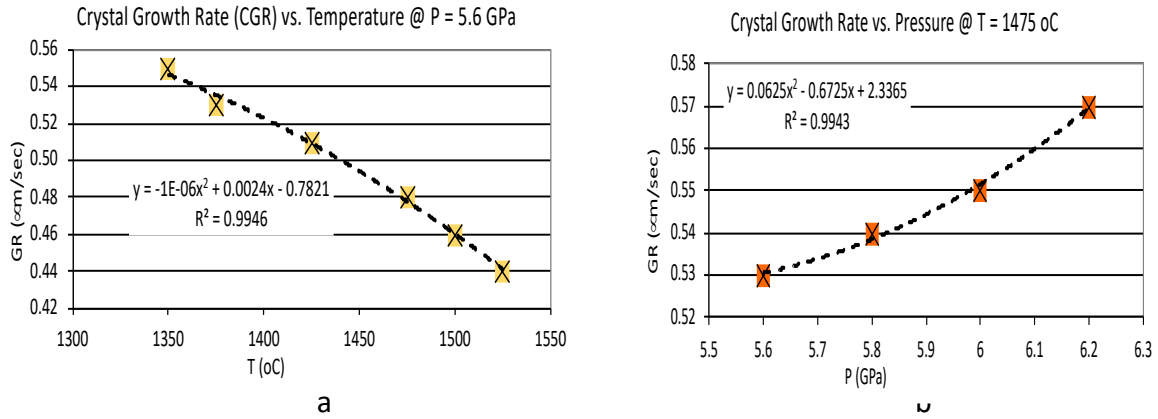

a b

Fig. 5.4. a and b – Dependence of diamond nucleation rate with temperature at constant pressure and with pressure at constant temperature

Tab. 5.5 – Experimental results and growth rate of diamond crystals

P	T	t	Md	Particle Size Distribution (ct)											d-avg	GR
(GPa)	(°C)	(sec)	(ct)	D252	D181	D151	D126	D107	D91	D76	D64	D54	D46	< D46	(∝)	(∝/sec)
5.6	**1350**	**260**	11.8	2.6	2.1	1.8	1.6	1.1	0.9	0.4	0.4	0.3	0.2	0.3	**142.75**	**0.55**
5.6	**1375**	**270**	13.1	3.1	2.6	2.0	1.6	1.0	0.9	0.4	0.4	0.2	0.2	0.6	**144.34**	**0.53**
5.6	**1425**	**280**	14.8	3.3	2.9	2.5	2.2	1.3	1.0	0.3	0.4	0.3	0.3	0.3	**142.14**	**0.51**
5.6	**1475**	**300**	9.2	1.9	2.0	1.7	1.3	0.7	0.5	0.2	0.3	0.2	0.2	0.3	**143.36**	**0.48**
5.6	**1500**	**300**	6.4	1.3	1.6	1.3	0.9	0.5	0.4	0.1	0.1	0.1	0.1	0.1	**138.58**	**0.46**
5.6	**1525**	**300**	3.6	0.4	0.7	0.9	0.7	0.4	0.3	0.1	0.1	0.0	0.0	0.1	**131.32**	**0.44**
5.6	**1550**	**300**	0.0												**0.00**	**0.00**

P	T	t	Md	Particle Size Distribution (ct)											d-avg	GR
(GPa)	(°C)	(sec)	(ct)	D252	D181	D151	D126	D107	D91	D76	D64	D54	D46	< D46	(∝)	(∝/sec)
5.6	**1475**	**300**	11.2	4.6	1.8	1.4	1.2	0.8	0.7	0.2	0.2	0.1	0.1	0.1	**159.15**	**0.53**
5.8	**1475**	**300**	26.7	12.2	4.0	2.9	2.6	1.6	1.6	0.5	0.5	0.3	0.3	0.3	**163.16**	**0.54**
6.0	**1475**	**300**	31.1	13.1	4.4	3.5	2.9	2.0	2.0	0.9	0.9	0.6	0.3	0.6	**166.11**	**0.55**
6.2	**1475**	**300**	35.3	14.2	5.0	4.0	3.4	2.5	2.5	0.9	0.9	0.6	0.6	0.6	**170.41**	**0.57**

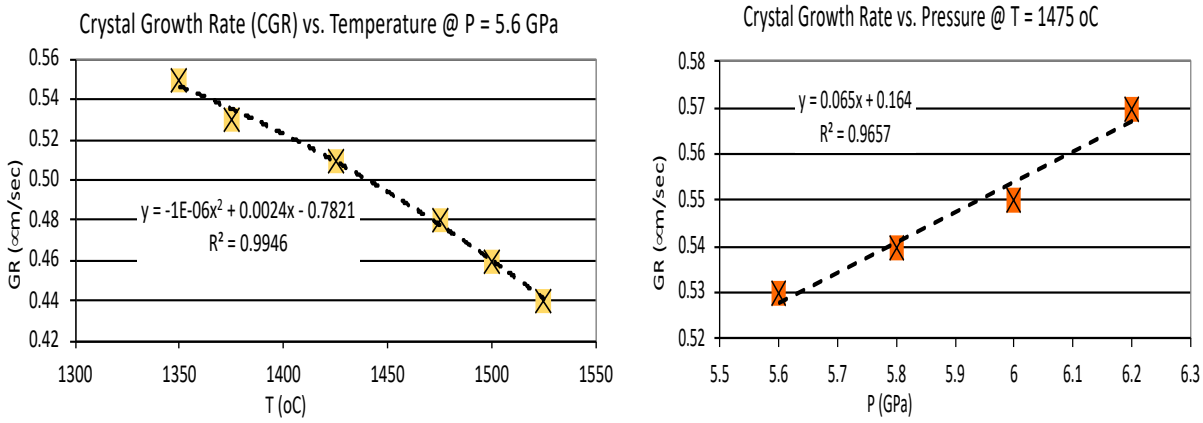

a b

Fig. 5.5. a and b – Dependence of growth rate of diamond with temperature at constant pressure and with pressure at constant temperature

Table 5.6 – X-ray diffraction phase analysis results on graphite-cobalt specimens reacted under different pressure-temperature conditions

Exp. Conditions				XRD phase analysis	Remarks
G-Co mass ratio	P (GPa)	T (^{o}C)	t (sec)		
G/Co = 1/1	5.6	1450	300	Graphite; Diamond; Co (c.f.c.)	
G/Co = 1/1	4.8	1350	300	Graphite; Co (c.f.c.)	
G/Co = 1/1	5.6	1450	300	Graphite (hexagonal)	after Co removal
G/Co = 1/1	4.8	1350	300	Graphite (hexagonal)	from reacted specimen

Tab. 6.1 – Nature and content of Co impurity in diamond crystals synthesized under different pressure-temperature conditions

P (GPa)	T (^{o}C)	t (sec)	Co Phase	Co wt %
5.6	1375	260	fcc-Co	1.47
5.6	1425	270	fcc-Co	0.74
5.6	1475	280	fcc-Co	0.33
5.2	1375	300	fcc-Co	2.28
5.6	1525	300	fcc-Co	0.22
6.0	1475	300	fcc-Co	0.54

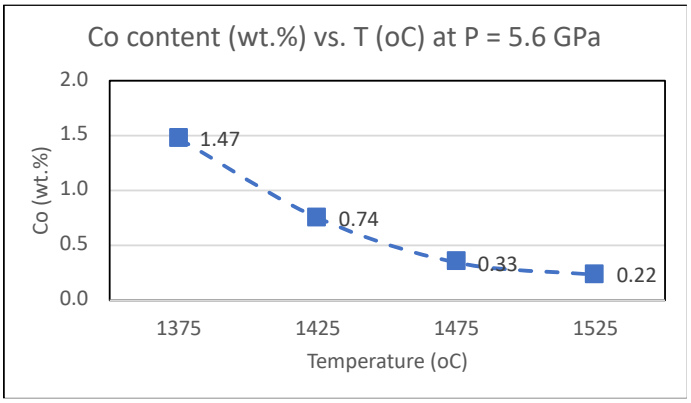

Fig. 6.1 – Dependence of Co content (%) with temperature at constant pressure

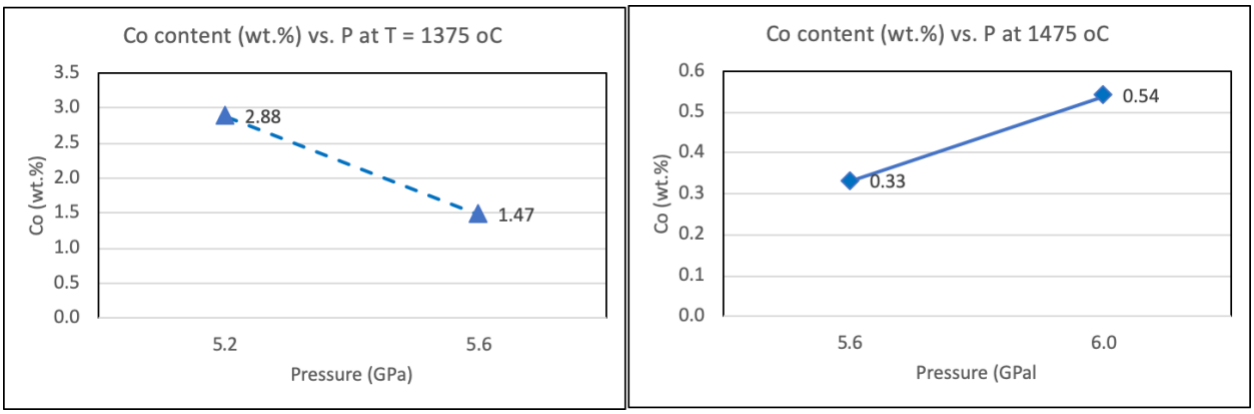

a b

Fig. 6.2 – Dependence of Co content (%) with temperature at constant pressure (a), and with pressure at constant temperature (b)

Tab. 6.2 – Morpho-structural characteristics of synthesized diamond crystals under different pressure-temperature conditions

P (GPa)	T (°C)	t (sec)	Size (∝m)	Morpho-structural characteristics of diamond crystals
5.6	1375	600	297-250	A-type crystal: majority B-type crystals: small number
5.6	1425	600	250-297	A-type crystals: large number B-type crystal: large number; C-type: relativ small numbe
5.6	1475	600	250-297	B-type crystals: approx. half C-type crystals: approx hallf
5.6	1525	600	250-297	C-type crystals: majority B-type crystals: reduced number
5.2	1375	600	250-297	Stratified grown black crystals; graphite layer alternating with diamond layers; A-type crystals: v. small numbers
6.0	1475	600	250-297	D-type crystals: large number multi-crystalline aggregates & macles: large number

Tab. 6.3 – Dependence of toughness index of synthesized diamond crystals with temperature at constant pressure (P = 5.6 GPa)

P (GPa)	T (°C)	t (sec)	Size	TI (%)
5.6	1375	600	250-297	13
5.6	1425	600	250-297	18
5.6	1475	600	250-297	29
5.6	1525	600	250-297	55

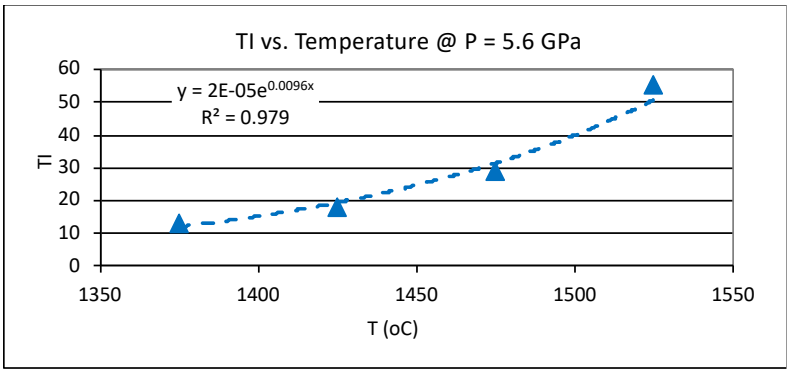

Fig. 6.3 – Dependence of toughness index of synthesized diamond crystals with temperature at constant pressure (P = 5.6 GPa)

Tab. 6.4 – Toughness index of synthesized diamond crystals with temperature at constant pressure

P (GPa)	T (°C)	t (sec)	Size	TI (%)
5.2	1475	600	250-297	
5.4	1475	600	250-297	65
5.6	1475	600	250-297	29
6.0	1475	600	250-297	15

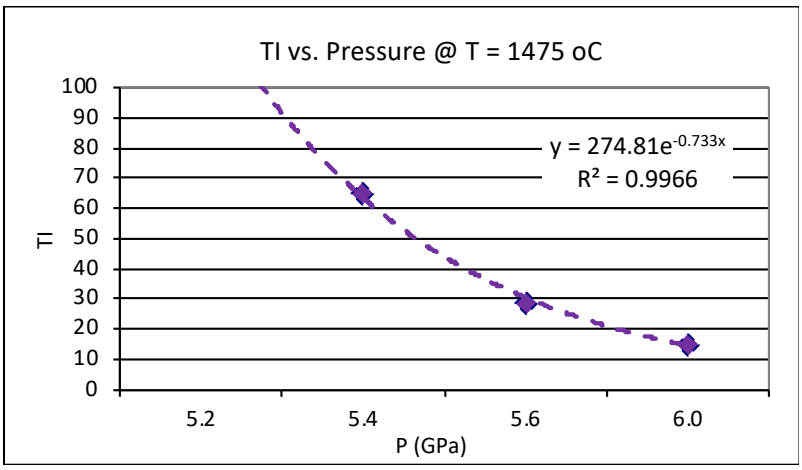

Fig. 6.4 – Dependence of toughness index of synthesized diamond crystals with pressure at constant temperature